

## Transient events in the near-nuclear regions of AGNs and quasars as the sources of the proper motion imitations

**I. M. Khamitov<sup>\*1,2</sup>, I. F. Bikmaev<sup>1,2</sup>, M. R. Gilfanov<sup>3,4</sup>, R. A. Sunyaev<sup>3,4</sup>,**  
**P. S. Medvedev<sup>3</sup>, M. A. Gorbachev<sup>1,2</sup>**

<sup>1</sup>*Kazan Federal University, Kazan, Russia*

<sup>2</sup>*Tatarstan Academy of Sciences, Kazan, Russia*

<sup>3</sup>*Space Research Institute of Russian Academy of Sciences, Moscow, Russia*

<sup>4</sup>*Max-Planck Institute for Astrophysics, Garching, Germany*

Received September 21, 2023

**Abstract** — This paper is an extension of the Khamitov et al. (2022) study in terms of cataloging and astrophysical interpretation of imitation of significant proper motions in galaxies with active nuclei and quasars which have been measured using data from the GAIA space observatory. We present a sample of SRG/eROSITA X-ray sources located in the eastern Galactic hemisphere ( $0^\circ < l < 180^\circ$ ), with significant proper motions according to GAIA eDR3 measurements and whose extragalactic nature has been confirmed. The catalog consists of 248 extragalactic sources with spectroscopically measured redshifts. It includes all objects available in the Simbad database and matched to the identified optical component within a radius of 0.5 arcsec. Additionally, the catalog includes 18 sources with the spectral redshift measurements based on observations at the Russian-Turkish 1.5-m telescope RTT-150, Khamitov et al. (2022). The sources of the catalog are AGNs of various types (Sy1, Sy2, LINER), quasars, radio galaxies, and star-forming galaxies. The imitation of significant proper motions can be explained (previously known in astrometry as the VIM effect) by the presence of transient events on the line of sight in the field of view of AGN nuclei and quasars (within the GAIA resolution element). Such astrophysical phenomena may be the supernovae outbursts, tidal destruction events in AGNs with double nuclei, variability of large-mass supergiants, the presence of O-B associations in field of view of variable brightness AGN, etc. A model of flares with a fast rise and exponential decay profile allows to describe the variable positional parameters of most similar sources observed in GAIA. This cross-matching approach of the X-ray source catalogs of the SRG/eROSITA observatory and the optical catalog of the GAIA observatory can be used as an independent technique for detecting transient events in the neighborhood of AGN core (on scales of several hundred parsecs in the picture plane).

**Keywords:** X-ray sources, active galaxy nuclei, proper motions, catalog, transient events

### INTRODUCTION

The Gaia Collaboration et al. (2022), Souchay et al. (2022), Makarov & Secrest (2022), and Khamitov et al. (2022) presented in their papers lists of quasars - point-like objects, not resolved by the GAIA satellite but are extragalactic according to their observed redshifts, with large peculiar motions according to the GAIA astrometric measurements (Gaia Collaboration et al., 2021). In the extragalactic sources reference frame the observed amplitudes of proper motions correspond to displacements of matter with velocities exceeding the speed of light by tens and hundreds of times. The imitation of the observed proper motions of AGN and quasars is most likely a manifestation of the well-known VIM effect, variability-induced-movers, caused by source variability. Initially, a method for investi-

gating the implications of this effect was developed to analyze data of the space astrometry mission Hipparcos (Wielen, 1996). It was focused to search for double stars in unresolved images, assuming that either one of the sources has variable brightness or there is a noticeable orbital motion in the binary system over the lifetime of the mission. The unprecedented positional accuracy, all-sky depth of the survey, and long duration of stable performance of the GAIA mission led to detection of numerous VIM occurrences in extragalactic sources in the optics. The observed amplitudes of proper motions of AGN and quasars are several orders of magnitude larger than the cases when the changes in the photocenter occur due to large-scale changes in the accretion disk and dust torus surrounding the central black hole, or due to the influence of primary gravitational waves or anisotropic expansion of the Universe, as well as mi-

---

\* e-mail: irek\_khamitov@hotmail.com

crolensing (see Souchay et al. (2022) and references therein). In Popović et al. (2012) it is considered a model of a relativistic disk around a supermassive black hole (SMBH) including perturbations, leading to the brightening of a part of the disk and, consequently, to the displacement of the photocenter position. It was shown that the result of the rearrangement of the internal structure of the accretion disk can produce a photocenter offset of up to several mas (milli arcsec) in the GAIA data, but only for bright quasars at low redshifts. Also in this paper, the proposed model was applied to long-term observations of a sample of 20 quasars exhibiting significant photocenter variability. For the cases of SDSS J121855.80+020002.1 and Mrk 877, the model was insufficient and the possibility of supernovae exploding very close to the central AGN source and a possible indication of a kpc (pc) scale binary SMBH was discussed. In Makarov & Secrest (2022) a comparison of the MIRAGN and GAIA eDR3 catalogs resulted in a list of 44 candidate double and multi-system quasars with proper motions and 4 known gravitationally-lensed systems. It is suggested that many proper motion quasars may be closer unresolved double systems exhibiting the VIM effect, and a smaller fraction may be random coincidences with foreground stars causing weak gravitational lensing. The Pierce et al. (2023) shows that galaxy interactions are the dominant mechanism for triggering quasar activity in the local Universe. It is shown that the host galaxies of type II quasars in  $\sim 65\%$  show morphological features corresponding to mergers or encounters of galaxies. In contrast to the idea that quasars are triggered at galaxy merger peaks, when two nuclei coalesce, and only become visible post-coalescence, most of the morphologically perturbed type II quasars in the Pierce et al. (2023) sample are observed in the pre-coalescence phase ( $61^{+8}_{-9}\%$ ).

The detection of AGN with source position offset on scales up to several *mas*, measured from VLBI radio data relative to GAIA measurements in the directions along and opposite to the jets, indicates the presence of strong extended optical jet structures in these systems on parsec scales (Kovalev et al., 2017). These studies have shown that to explain the VLBI-GAIA bias the radiative sizes of the required strong optical jet should be at least 20-50 pc (Plavin et al., 2019). Differential brightness variations in jets of this type can lead to the observed VIM effect in GAIA data. Optically bright jets with ultrarelativistic proper motions were also observed in the nearest strong radio galaxy M87 (Biretta et al., 1999), where the Hubble telescope was able to observe motions of details in the image of jets with apparent velocities up to 6-8 light speeds. Souchay et al. (2022) briefly investigated both of the above scenarios and concluded that radio jet ac-

tivity cannot be the main factor affecting the apparent proper motion in quasars in optics.

In Khamitov et al. (2022) we report a sample of 502 extragalactic X-ray sources detected by the eROSITA telescope (Predehl et al., 2021) of the space observatory Spectrum-Roentgen-Gamma (Sunyaev et al., 2021) in the eastern galactic hemisphere, for which the Russian consortium of eROSITA telescopes is responsible for data processing ( $0^\circ < l < 180^\circ$ ), and for which the GAIA satellite has measured significant values of proper motions. Most of these sources belong to extended optical sources according to GAIA, and only about 1.5% of them are stars in our Galaxy. Using the Simbad database, it has been shown (Khamitov et al., 2022) that an extragalactic nature is confirmed for about half of these 502 sources. For the remaining half, additional spectroscopic observations are required to estimate their redshifts and to do their optical identification. This work is carried out by the authors of the paper - based on observations on the 1.5-meter optical Russian-Turkish telescope RTT-150 (TÜBITAK National Observatory, Antalya, Turkey), the extragalactic nature of 18 sources has already been previously confirmed from the second half of the Khamitov et al. (2022) list. In the current paper we present a catalog of 248 X-ray sources of eROSITA discussed in Khamitov et al. (2022) for which spectroscopic redshift determinations and optical classification are available. The catalog includes all objects available in the Simbad database that match the identified optical component within a radius of 0.5 arcsec, and from spectral observations performed with the RTT-150 telescope. An additional source selection criterion was their absence among GAIA DR3 objects with spurious time-series signal by position related to the time-dependent angle of scanning of objects by GAIA detectors (Holl et al., 2023). The catalog can be used in the future to search for and analyze the origin of GAIA significant proper motions of extragalactic objects from which formally follow the motions of matter in these sources with significant excesses of the speed of light.

In the following tables we provide an additional list of 12 quasars, 2 blazars, and 4 radio galaxies from the X-ray catalog of the SRG/eROSITA telescope, which have large peculiar motions according to the GAIA satellite data. Many blazars and part of quasars demonstrate the presence of strong optical jets.

However, our catalog of extragalactic objects with large proper motions includes not only quasars or strong AGNs and radio galaxies, but also other systems. For example, galaxies with strong star formation, the nature of which is hardly related to the presence of powerful optical jets, are of independent interest. It may well turn out that in these objects with frequently exploding supernovae, the measured large

apparent velocities of the central region of the galaxies are explained by a displacement of the galaxy's photocenter due to a simultaneously recorded bright supernova outburst at an appreciable distance from the galaxy's brightness center. It is possible that for the same reason (bright supernova outburst in the surrounding galaxy) the brightness center of the galaxy with AGN can be shifted for a while, which is presented in the results of GAIA observations.

The phenomenon of tidal destruction of stars by a supermassive black hole can also make the accretion disk around the black hole brighter than the whole galaxy for a distant observer for a time of the order of a year. Due to many reasons it will result in a shift of the measured photocenter. Moreover, for double systems it will lead to essential values. It is obvious that at such strong energy generation the bright optical jets with ultrarelativistic velocities can sometimes be formed.

Below we have categorized the objects in our catalog by type so that professionals can more quickly find the objects they are interested in. The imitation of strong proper motion of extended extragalactic objects detected by GAIA may lead to interesting and unexpected conclusions about the physical processes resulting in such imitation.

To describe the observational parameters of the GAIA catalog - astrometric noise (astrometric\_excess\_noise) and the ratio of the total source displacement to this noise, we considered the effect of a FRED profiled flare on the position of the photocenter which took place at a given distance from a galaxy core.

## CATALOG

Spectroscopic redshift estimations are available for 248 objects. The catalog is presented as one common identification Table 1 and 9 Tables 2 - 10 with X-ray characteristics, classified by common object types: quasars - 11 sources; blazars - 2 sources; radio galaxies (Galaxy R) - 4 sources; Seyfert type 1 galaxies - 106 sources; Seyfert type 2 galaxies - 32 sources; LINER type AGNs - 11 sources; AGNs of undetermined type - 25 sources; star forming galaxies (SF) - 15 sources and undetermined type galaxies - 42 sources. The identification table is ordered by right ascension, while within the X-ray tables, objects are listed in descending order of proper motion modulus according to GAIA eDR3 data.

The identification table has 9 columns: 1) SRG/eROSITA catalog identification number; 2) GAIA eDR3 catalog identification number; 3) RA (J2000.0); 4) DEC (J2000.0); 5) proper motion module with its measurement error in mas units; 6) redshift; 7) source type; 8) identification in the Simbad

database; 9) reference code for the article from which the redshift information was received.

The X-ray characterization tables have 9 columns: 1) RA (J2000.0); 2) DEC (J2000.0); 3) magnitude in the G band (Gaia eDR3); 4) proper motion modulus in mas units; 5) logarithm of the ratio of the X-ray flux  $F_X$  from eROSITA data in the range 0.3–2.3 keV to the optical flux  $F_{opt}$  in the G band from Gaia eDR3 data; 6)  $X_v$  X-ray variability, defined as the ratio between the maximum and minimum flux values in the 4 eROSITA surveys without taking into account the flux measurement error; 7) X-ray luminosity from eROSITA data in the range 0.3–2.3 keV in its own reference frame without correction for internal absorption and absorption in the Galaxy<sup>1</sup>; 8) redshift; 9) lower estimation of the largest optical luminosity of the transient event falling within the GAIA catalog interval (see Appendix 1).

## TRANSIENT EVENTS AS SOURCES OF PROPER MOTION IMITATION IN AGN.

Within the GAIA resolution element (60 mas) a transient event comparable in flux to the optical radiation of the AGN itself can be captured together with the AGN image. In this case, due to a noticeable brightness variations of the transient event, the AGN photocenter registered by GAIA will vary in time and, consequently, a spurious signal of the AGN proper motion will be observed. Thus, in the projection onto the picture plane at a radius of 60 mas from the apparent center of the AGN, there may be an additional sufficiently bright source located inside the host galaxy even at significant distances from the active nucleus. Such a source is most likely in the foreground because of the strong absorption near the core.

The distribution of the catalog's AGNs depending on the object type in the plane of astrometric noise ( $\epsilon$ , astrometric\_excess\_noise) and the ratio of the total source displacement to the astrometric noise ( $2.8\mu/\epsilon$ ) according to the GAIA data is shown in Fig.1. The astrometric noise parameter in GAIA is determined by the discrepancy between the source coordinates in the 5-parameter model of the global measurements and the photocenter measured directly on the base of individual observations as the weighted center. For nearby galaxies ( $z < 0.3$ ), the discrepancies are affected by the asymmetric structure of the galactic component due to the tracing of the GAIA detector windows at different angles. It is important that our catalog sources show no spurious signal of the temporal position dependence associated with the scan angle (Holl et al., 2023). In addition, investigations of the offsets in the positions of

---

<sup>1</sup>For the calculation we assumed the standard cosmological model  $\Lambda$ CDM with the following parameters:  $\Omega_m = 0.3$ ,  $\Omega_\Lambda = 0.7$ ,  $H_0 = 70$  km/s/Mpc

VLBI to the GAIA photocenters in AGN have shown that in 73% of the cases of significant offsets there were coincidences with the direction of the radiojet. This indicates that the host galaxy does not play an important role in the detected offsets and, therefore, argues in favor of a symmetric optical brightness distribution in the near-nuclear region (Plavin et al., 2019). Obviously, the discrepancies associated with a transient event will take place in the direction of the photocenter of the source in the absence of a transient to the position of the latter. Thus, for cases of close and bright AGN of the catalog, the level of astrometric noise not related to the VIM effect due to the transient event can be estimated from GAIA data by the cross-directional deviations of the photocenter with respect to the proper motion vector. The dotted lines are the modeling results  $(\mu, \epsilon)$  for the case when the transient brightness variations corresponds to a fast rise and exponential decay profile (FRED) that occurred at different apparent distances of the transient from the nucleus ( $X_T$ ): black line - 60 mas, red line - 30 mas (see Appendix 1). The distributions are constructed for the case of the ratio of the peak transient flux to the flux from the nucleus  $R_0 = 1$ , the fast rise parameter  $\sigma = 10^d$ , and the decay factor  $\alpha = 111^d$ , which corresponds to the decay  $Co^{+56}$  characteristic of supernova explosions.

The considered fitting of the observed parameters  $(\mu, \epsilon)$  by FRED flares is a multi-parameter problem that also depends on the cadence of source observations in GAIA. Using optical light curves of GAIA sources from the AGN catalog with significant proper motions will provide model parameters. Besides, the proposed model does not consider the spectral energy distribution (SED) of flares and its evolution with time. The necessity of SED including into the analysis becomes relevant depending on the redshift, since as the distance to the object increases, the recorded with the GAIA detectors bandwidth will correspond to more and more short-wavelength regions of the flare electromagnetic emission. To detailed modeling with SED it is required the complete source information of GAIA eDR3 catalog (photometric light curves and positional data) for the entire observation period. But a series of qualitative conclusions can already be drawn:

1. On the GAIA light curves, in those cases where the maximum of the supernova outburst took place during the catalog interval, a relatively sharp and short-term brightness variation - an outlier - should be observed. The transient position with respect to the nucleus corresponds to the direction of the proper motion vector. But in cases where the observations were performed on the fading branch of the flare, the slow decrease in brightness can be interpreted as an intrinsic vari-

ability of the nucleus. The position of the transient is opposite to the direction of the proper motion vector with a slow decrease in modulus in contrast to the impact of the internal variability of the nucleus structure, which GAIA does not detect. Thus, it is possible to limit the time domains of the location of the flare maximum moment - before or during the GAIA catalog, i.e., horizontal or vertical solutions of the model.

2. Using new astrometric data the reversal of the sign of the AGN apparent proper motion can be measured for the case of the flare maximum located within the GAIA eDR3 catalog. The change in sign will take place in the subsequent GAIA observing period, when only the fading branch of the flare is observed.
3. In galaxies with intense star formation, LINER, and radio galaxies, the transient event is observed at distances of at least 30 mas in the model with  $R_0 = 1$ . For models with  $R_0 < 1.0$ , or  $\alpha < 111^d$  this lower limit is even higher. This limitation is on the one hand explained by the strong dust absorption in the near-core region in star-forming and LINER galaxies, but on the other hand it is an indirect indication that regions with a high-energy transient event should be closely related to the core activity.
4. The Pierce et al. (2023) shows that galaxy interactions are the dominant mechanism for triggering quasar activity in the local Universe. It is shown that host galaxies with type II quasars in  $\sim 66\%$  demonstrate morphological features corresponding to mergers or encounters of galaxies. In contrast to the idea that quasars are triggered at galaxy merger peaks, when two nuclei merge, and become visible only after complete merging, most morphologically perturbed type II quasars in the sample from the Pierce et al. (2023) paper are observed at a stage prior to the complete merging phase ( $61_{-9}^{+8}\%$ ). Thus, the quasars in our sample with significant proper motions are very likely to be double nuclei within 60 mas or on the order of a few hundred parsecs away. For quasar SRGeJ131118.5+463502, the lower estimation of the luminosity of the transient event within the GAIA catalog interval ( $L_T$ ) is about  $1.3 \times 10^{44} erg/s$  (in Fig. 1 in the panel with quasars, this source is highlighted by a blue circle). This luminosity exceeds the maximum luminosity values for supernova events and is a candidate for a tidal disruption event (TDE) in a double-core system. At the picture plane, the two SMBHs are separated by an angular distance of

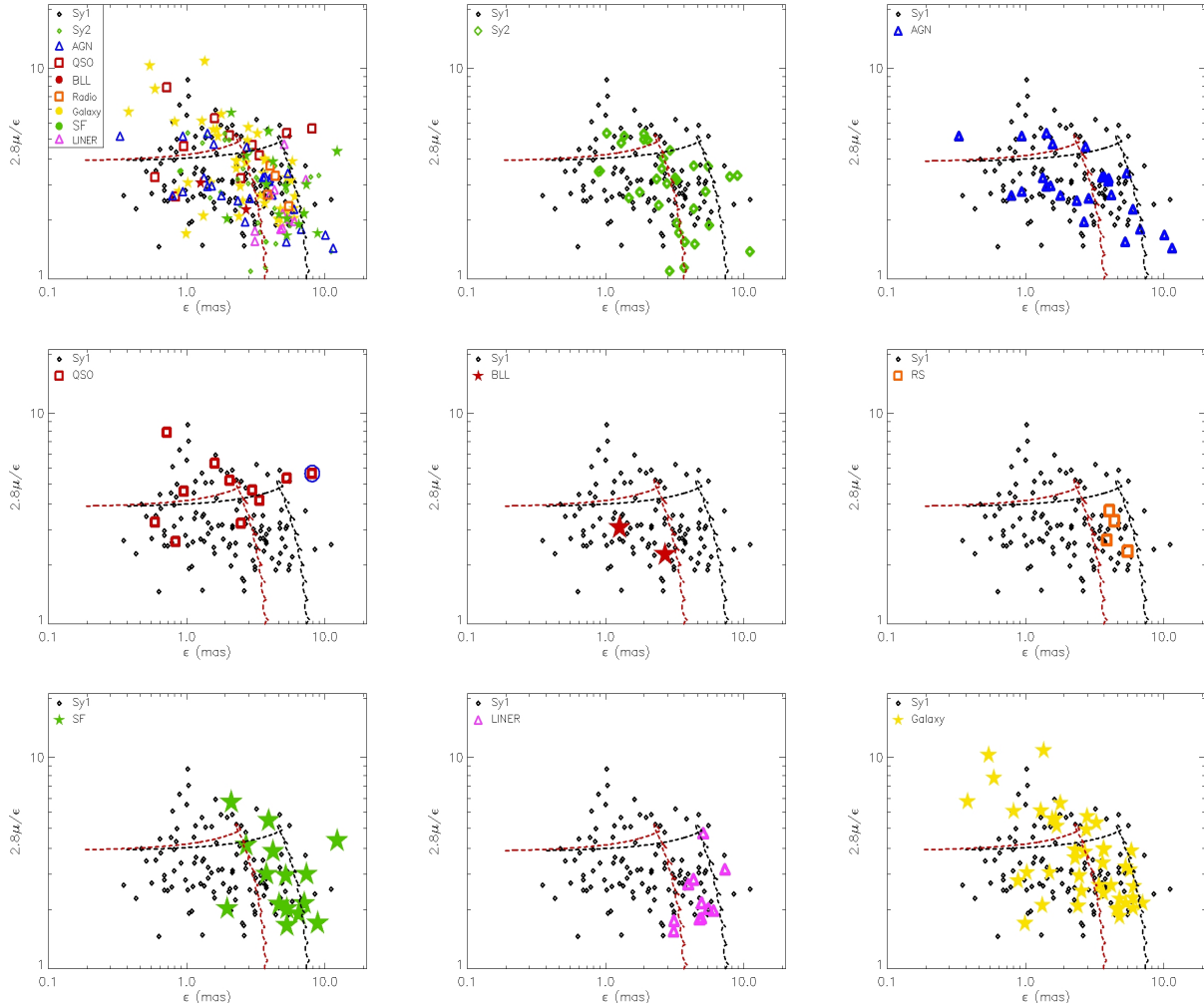


**Fig. 1.** Source type distribution in the plane  $\epsilon - 2.8\mu/\epsilon$ .

at least 60 *mas*, which at redshift  $z=0.271$  corresponds to distances of the order of 250 parsecs. Of course, to model the TDE it is necessary to use a more sophisticated dependence than FRED, involving an exponential function at large times after the flare maximum(van Velzen et al., 2021). The strongly variable AGNs found in the eROSITA catalog (Medvedev et al., 2022) may exhibit similar phenomena in the registration of their proper motion in the GAIA catalog. The VIM effect will manifest itself in the period when this variability has been detected, i.e., using GAIA data only in the period 2020-2022.

5. To explain the apparent proper motion via a transient event in the neighborhood of the AGN nucleus, there are cases with apparent proper motions of gas ejections similar to those observed in the nearest strong radio galaxy M87 (Biretta et al., 1999). The Hubble telescope made it possible to observe moving details in the image of a jet with apparent proper motions ( $\mu_{jet}$ ) on the order of 20 *mas/yr* at a relative brightness of  $R \sim 0.01$  with respect to the optical core of M87. The model considered in Appendix 1 with linear transient motion based on the GAIA-measured proper motions of blazars from the Table 7 gives estimates of the jet brightness, at 20 *mas/yr* proper motions of the jet, on the order of 10% of the core brightness ( $R = 0.1$ ). This value is an order of magnitude higher in relative luminosity compared to the optical details of the jets in M87, and the apparent magnitudes of the objects themselves are at the limit of detection by the GAIA detectors. But, on the other hand, in the experience of the M87, the GAIA resolution element may capture a large group of more faint details of the jet. Together, they can provide a higher ratio ( $R = 0.1$ ).

The presence of an optical jet in these objects may well explain the apparent proper motions. The presence of a flare in the neighborhood of the nucleus is not excluded in the cases of blazars as well. The use of astrometric trajectory from GAIA data allows us to separate the case of relativistic jet motion from a strong transit event. In the second case, variations in the position of the source will resemble the light curve of the flare (Fig.4,5), as observed, for example, in the Kepler Observatory data in the search for double unresolved systems (Makarov & Goldin, 2016).

6. AGNs of undetermined type have a clear binary distribution at  $2.8\mu/\epsilon$ . This behavior is also evident in the Sy1 and Sy2 distributions. Combining sources of this type gives maximum values:

$2.6 \pm 0.7$  and  $4.7 \pm 0.5$ . It should be noted that the larger value is approximated by the exponential decay parameter characteristic of supernova events.

7. In the case of galaxies where the luminosity of the nucleus is not so high, in some cases the apparent proper motions can be modulated by long-period variations in the luminosity of stellar objects. For example, in the well-known double system of our Galaxy  $\eta$  Carinae, quasi-periodic luminosity variations of several orders of magnitude over 5 years, reaching luminosity up to  $10^{39}$  erg/s, have been observed (Damineli, 1996). Such cases can be determined by examining the GAIA catalog on different time samples, separated by several non-overlapping years. They will demonstrate long-period proper motion variability.
8. For tidal disruption events in the gravitational field of a supermassive black hole, initially the photocenter must not coincide with the nucleus. These can be double core cases. At core luminosities below  $10^{40}$  erg/s, the initial offset of the photocenter can be provided by stellar O-B associations whose integral optical luminosity can be comparable to the core luminosity.
9. If our astrophysical interpretation of the proper motion imitation in the GAIA data is correct, then after the brightness of the transient event drops below the GAIA photometric threshold the extragalactic sources will be observed at the permanent positions in subsequent GAIA measurements. Or the directions and amplitudes of the spurious proper motions will change, in case new transient events occurred in these AGNs during the next GAIA scans in subsequent mission periods, after 2017.

## COMPARISON WITH THE GNT CANDIDATES CATALOG

Kostrzewska-Rutkowska et al. (2018) presented a catalog of about 480 candidates for transient events in the near-nuclear regions of galaxies detected from GAIA photometric data and the SDSS DR12 galaxy catalog (GNT catalog). Among the spectrally confirmed sources, two matches with GNT were found: SRGeJ143701.5+264019 and SRGeJ151721.7+465812. The light curve of the source SRGeJ143701.5+264019 known as a quasar is shown in Fig.2. The data corresponding to the GAIA eDR3 catalog period is indicated with red circles (vertical dashed line is the upper boundary of the catalog). A monotonic rise

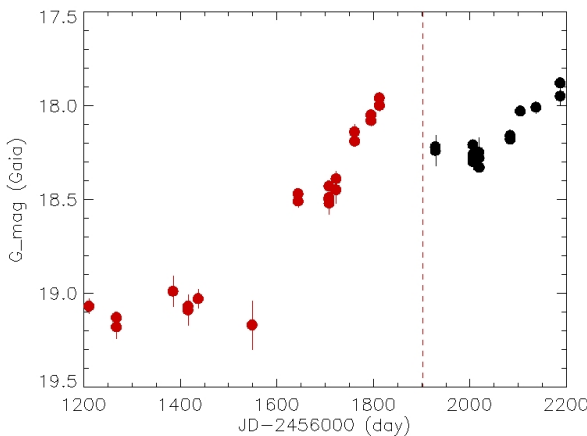


**Fig. 2.** Optical light curve of SRGeJ143701.5+264019 (quasar). Red circles show data corresponding to the period of the GAIA eDR3 catalog.

in brightness is observed which continued even after the end of the GAIA eDR3 catalog with an approximately twofold drop in flux between 1800 and 2000 days on the graph. To obtain the flare profile the detailed positional information is required. The SRGeJ151721.7+465812 light curve has a completely different appearance where a flare with a FRED profile definitely stands out. The light curve is shown in Fig.3 and the green dashed line represents the fit of the flare with model parameters:  $t_0 = 745^d$ ,  $R_0 = 2.6$ ,  $\sigma = 15^d$ ,  $\alpha = 111^d$ . The proper motion ( $17.63 \pm 2.3 \text{ mas/yr}$ ) and astrometric noise (12.2 mas) measured in GAIA, together with the flare parameters, are consistent with a transient distance from the core of  $X_T \sim 80 \text{ mas}$ . Using the source redshift  $z = 0.154$  determined from the RTT-150 spectral data, we obtain that in the object reference frame the transient event took place at a distance of  $\sim 214 \text{ pc}$ . An estimation of the luminosity of the flare at maximum corresponds to  $L_{max} = 2.2 \times 10^{43} \text{ erg/s}$ , which together with the exponential decay indicates that a Supernova event has occurred.

## CONCLUSION

The IMITATION of significant and high proper motions of AGN and quasars (identified by the SRG/eROSITA telescope as sources of X-ray emission) detected by GAIA measurements may be a manifestation of classical transient astrophysical events. These events take place in the near-nuclei regions (in the picture plane within the GAIA optical resolution element) of this type of extragalactic sources during long (several years) periods of high-precision measurements of their optical coordinates. Transient events result-

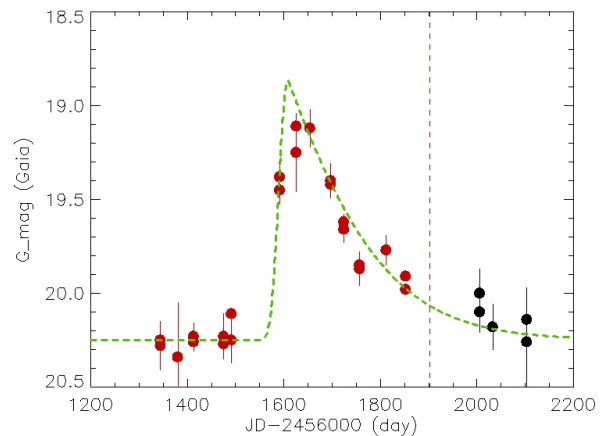


**Fig. 3.** Optical light curve of SRGeJ151721.7+465812 (star-forming galaxy). Red circles represent data corresponding to the period of the GAIA eDR3 catalog. Green dashed line shows the fit of the flare with FRED profile.

ing in displacements of AGN and quasar photocenters should have optical luminosities exceeding or comparable to the optical luminosities of AGN and quasars themselves. In our opinion, the most characteristic of the known astrophysical phenomena of such transient events are: supernovae outbursts, tidal disruption events in double SMBHs, high-amplitude long-term variations (increases or decreases) in the brightness of massive supergiant stars with outflowing envelopes and stellar winds of the  $\eta$  Carinae type, as well as the presence of stellar O-B associations in the field of view of AGN of variable brightness. This interpretation is more astrophysically driven than attempts to explain the significant proper motions of AGNs and quasars by more exotic effects.

This work is based on observations with the eROSITA telescope onboard the SRG observatory. The SRG observatory was built by Roscosmos in the interests of the Russian Academy of Sciences represented by its Space Research Institute (IKI) within the framework of the Russian Federal Space Program, with the participation of the Deutsches Zentrum fuer Luft- und Raumfahrt (DLR). The SRG/eROSITA X-ray telescope was built by a consortium of German Institutes led by MPE, and supported by DLR. The SRG spacecraft was designed, built, launched, and is operated by the Lavochkin Association and its subcontractors. The science data are downlinked via the Deep Space Network Antennae in Bear Lakes, Ussurijsk, and Baykonur, funded by Roscosmos. The eROSITA data used in this work were processed using the eSASS software system developed by the German eROSITA consortium and the proprietary data reduction and analy-

sis software developed by the Russian eROSITA Consortium. This research has made use of the SIMBAD database, operated at CDS, Strasbourg, France. The authors are grateful to TÜBİTAK, IKI, KFU, and the Academy of Sciences of the Tatarstan Republic for partial support in use of RTT-150 (Russian-Turkish 1.5-m telescope in Antalya).

The study was supported by a grant from the Russian Science Foundation N 23-12-00292.

18. S. van Velzen, S. Gezari, E. Hammerstein, N. Roth, S. Frederick, C. Ward, et al., *Astrophys. J.*, **908**, 4 (2021)
19. R. Wielen, *Astron. Astrophys.*, **314**, 679 (1996)

## REFERENCES

1. J. A. Biretta, W. B. Sparks, and F. Macchetto, *Astrophys. J.*, **520**, 621 (1999)
2. A. Damineli, *Astrophys. J. (Letters)*, **460**, L49 (1996)
3. Gaia Collaboration, A. G. A. Brown, A. Vallenari, T. Prusti, J. H. J. de Bruijne, C. Babusiaux, et al., *Astron. Astrophys.*, **649**, A1 (2021)
4. Gaia Collaboration, S. A. Klioner, L. Lindegren, F. Mignard, J. Hernandez, M. Ramos-Lerate, et al., *Astron. Astrophys.*, **667**, id.A148,31 (2022)
5. B. Holl, C. Fabricius, J. Portell, L. Lindegren, P. Panuzzo, M. Bernet, et al., *Astron. Astrophys.*, **674**, A25 (2023)
6. I. M. Khamitov, I. F. Bikmaev, M. R. Gilfanov, R. A. Sunyaev, P. S. Medvedev, M. A. Gorbachev, et al., *Astronomy Letters*, **48**, 724 (2022)
7. Z. Kostrzewska-Rutkowska, P. G. Jonker, S. T. Hodgkin, Ł. Wyrzykowski, M. Fraser, D. L. Harrison, et al., *Mon. Not. R. Astron. Soc.*, **481**, 307 (2018)
8. Y. Y. Kovalev, L. Petrov, and A. V. Plavin, *Astron. Astrophys.*, **598**, L1 (2017)
9. V. V. Makarov and A. Goldin, *Astrophys. J. Suppl. Ser.*, **224**, 19 (2016)
10. V. V. Makarov and N. J. Secrest, *Astrophys. J.*, **933**, 28 (2022)
11. P. S. Medvedev, M. R. Gilfanov, S. Y. Sazonov, R. A. Sunyaev, and G. A. Khorunzhev, *Astronomy Letters*, **48**, 735 (2022)
12. J. C. S. Pierce, C. Tadhunter, C. Ramos Almeida, P. Bessiere, J. V. Heaton, S. L. Ellison, et al., *Mon. Not. R. Astron. Soc.*, **522**, 1736 (2023)
13. A. V. Plavin, Y. Y. Kovalev, and L. Y. Petrov, *Astrophys. J.*, **871**, 143 (2019)
14. L. Č. Popović, P. Jovanović, M. Stalevski, S. Anton, A. H. Andrei, J. Kovačević, et al., *Astron. Astrophys.*, **538**, A107 (2012)
15. P. Predehl, R. Andritschke, V. Arefiev, V. Babyshkin, O. Batanov, W. Becker, et al., *Astron. Astrophys.*, **647**, A1, 16 (2021)
16. J. Souchay, N. Secrest, S. Lambert, N. Zacharias, F. Taris, C. Barache, et al., *Astron. Astrophys.*, **660**, A16, 1 (2022)
17. R. Sunyaev, V. Arefiev, V. Babyshkin, A. Bogomolov, K. Borisov, M. Buntov, et al., *Astron. Astrophys.*, **656**, A132, 29 (2021)

## APPENDIX 1

*Determination of the brightness center in the case of a transient event.*

We have considered the variation of the total brightness center in time and "GAIA data" of two objects: a) quasi-stationary and flared for a short time (a year) with a given light curve; b) quasi-stationary and with apparent linear motion. The objects are considered as a point-like.

In both cases, the study can be reduced to a one-dimensional model. In the picture plane, we refer the coordinate center to the position of the active nucleus, i.e.,  $X_{AGN} = 0$ , and orient the X axis away from the AGN toward the transient event (TE). Obviously, the brightness center with the transient event at a distance  $X_T$  from the AGN position is determined as:

$$X_C = \frac{X_T F_T}{F_T + \langle F_{AGN} \rangle + \xi(t)}, \quad (1)$$

where  $\langle F_{AGN} \rangle$  is the average flux from AGN,  $F_T$  is the flux from TE recorded at a certain moment of time,  $\xi(t)$  is the stochastic variability of the core with respect to the mean value.

Consequently, there are two limit values of  $X_C$ . These are:

$$X_C = \begin{cases} X_T, & \text{if } F_T \gg F_{AGN} \\ 0, & \text{if } F_T \ll F_{AGN} \end{cases} \quad (2)$$

The second limit value is reached rather quickly, e.g., for a supernova event or a tidal disruption event. Consequently, for known values of proper motion ( $\mu$ ) measured in the GAIA catalog and the AGN flux estimation, the lower value of the largest transient flux in the GAIA observation interval can be estimated in TE cases:

$$F_T = \frac{\mu t_{gaia}}{X_T - \mu t_{gaia}} F_{AGN}, \quad (3)$$

where  $t_{gaia}$  is the time base of the GAIA eDR3 catalog, on the basis of which the proper motion of the sources was determined, i.e., 2.8 years. Since both sources are at the same distance, the fluxes can be replaced by the luminosities of the sources in the formula 3. By adopting a conservative constraint on the maximum possible value of  $X_T$  by the resolution element of the GAIA detector, i.e., 60 mas, the lower value of the transient luminosity was calculated. The results are summarized in tables 2-10 in the 9th column ( $L_T$ ).

In addition to the proper motion parameter, the GAIA catalog also provides the astrometric noise parameter  $\epsilon$  (astrometric\_excess\_noise). By introducing a new variable  $R$  as the ratio of TE fluxes to the average AGN flux and taking the ratio  $\xi(t)$  to the sum of TE and AGN fluxes on the time base of the GAIA catalog to be less than unity, and in fact in the time

interval when TE can be registered by Gaia detectors, (1) takes the form:

$$X_C = \frac{R}{R+1} X_T - \frac{R}{(R+1)^2} \xi'(t) X_T, \quad (4)$$

where  $\xi'(t) = \frac{\xi(t)}{\langle F_{AGN} \rangle}$ . The second term of the sum in (4), which has chaotic behavior, gives an additional small contribution to the astrometric noise, depending on the amplitude of the intrinsic relative variability of the core on the scale of the flare registration.

*The case of a quasi-stationary object and an object flared at a given distance.*

A simple model of the effect of a flare with a fast rise and exponential decay (FRED) profile that took place at some distance from the core ( $X_T$ ) was considered. The fast rise is provided by a Gaussian:

$$R_i = R_0 \times \begin{cases} e^{-(t_i - t_{peak})^2 / 2\sigma^2} & \text{if } t_i \leq t_{peak} \\ e^{-(t_i - t_{peak})/\alpha} & \text{if } t_i > t_{peak} \end{cases} \quad (5)$$

where  $t_{peak}$  is the moment of maximum flare flux,  $R_0$  is the ratio of TE and AGN fluxes at the moment  $t_{peak}$ ,  $\sigma$  is the standard deviation of the Gaussian,  $\alpha$  is the exponential decay parameter, and  $t_i$  are the moments of observations in the GAIA catalog, which are used in the model with some arbitrariness. According to the GAIA observatory sky scanning parameters, each source is observed 70 times on average during a 5-year survey of the entire sky, i.e., at least one measurement per 30 days. Thus, for modeling it was assumed that at least 39 photometric and positional measurements of extragalactic sources were carried out during the  $t_{gaia}$ .

Then, having estimated the position of the brightness center  $X_C$  by the formulas (4) and (5), the proper motion  $\mu$  and the standard deviation from the line  $\epsilon$  are calculated for all points by linear interpolation ( $\epsilon$  does not include the contribution from the stochastic variability of the core). Depending on the time offset ( $LAG$ ) of the flare maximum moment  $t_{peak}$  compared to the beginning of the GAIA survey, these discrete measurements will correspond to different parts of the flare. Two cases can be distinguished depending on the sign of  $LAG$ . First, at negative values, the maximum of the flare is within the survey period (Fig.4). Measurements of the brightness center before the flare will correspond to unbiased values regardless of the core variability, i.e., equal to zero. Second, with positive values, the maximum of the flare was before the beginning of the survey (Fig.5) and all measurements of the brightness center would be displaced. These examples do not take into account the intrinsic variability of the core brightness,  $X_T$  is 60 mas,  $R_0 = 1$ , and  $\sigma = 10^d$ .

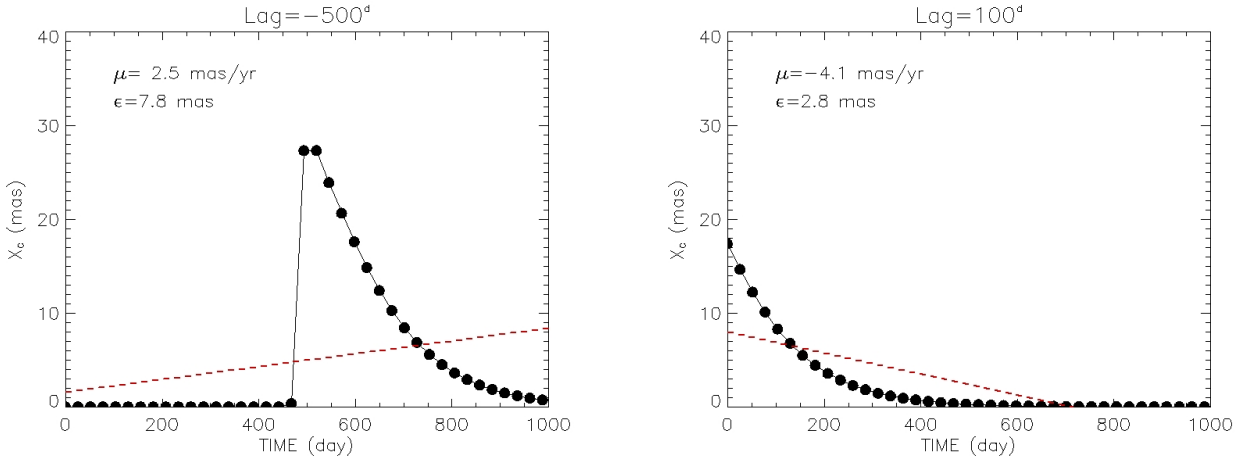


**Fig. 4.** FRED-profile flare that has taken place 500 days after the beginning of the survey. The dots show simulated measurements of the photocenter of the AGN with the flare at a distance  $X_T = 60 \text{ mas}$  from the nucleus ( $R_0 = 1, \alpha = 110^d, \sigma = 10^d$ ). The zero value on the x-axis corresponds to the beginning of the GAIA survey. We present estimates of proper motion and astrometric noise obtained by linear approximation of all the measurements of the photocenter.

The considered fitting of the observed parameters  $(\mu, \epsilon)$  by FRED flare is a multiparametric problem. Indeed, decreasing the parameter  $X_T$  or decreasing the parameter  $R_0$  leads to a horizontal shift of the solutions towards a decrease in  $\epsilon$  (Fig.6,7). While decreasing the exponential decay parameter  $\alpha$  leads to a vertical shift towards a decrease in the ratio of proper motions to astrometric noise (Fig.8). The horizontal branches of the model estimates correspond to periods when the maximum of the transient event flux occurred before the beginning of the GAIA catalog, while the vertical part corresponds to moments when the flare took place within the time interval covered by the GAIA catalog. Smaller  $\epsilon$  values on the horizontal branch correspond to larger *LAG* parameters, and on the vertical curve smaller  $2.8\mu/\epsilon$  values correspond to smaller *LAG* values.

Besides the considered case with a quasi-stationary object and an object flaring at a given distance, there is a possible case of two quasi-stationary objects (distance between the objects  $X_T$ ), in the neighborhood of one of which a transient event occurs. In this case, (1) takes the form of:

$$X_C = \frac{X_T F_2 + X_T F_T}{F_1 + F_2 + F_T} \quad (6)$$

where  $F_1$  and  $F_2$  are the fluxes of the first object and, respectively, the second object in the neighborhood of which the transient event took place. Introducing the

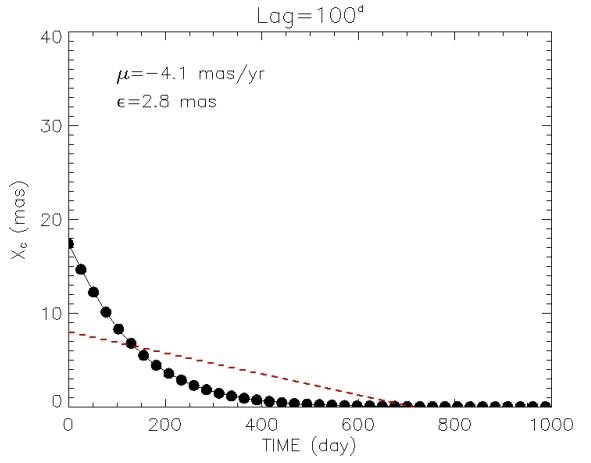


**Fig. 5.** Photocenter variations in a case of FRED-profile flare that took place 100 days before the GAIA survey (model parameters:  $X_T = 60 \text{ mas}$ ,  $R_0 = 1$ ,  $\alpha = 110^d$ ,  $\sigma = 10^d$ ). The negative value of the proper motion in the one-dimensional model corresponds to the direction from the flare toward the nucleus.

variable  $R = \frac{F_T}{F_1 + F_2}$ , (6) takes the following form:

$$X_C = \frac{X_0 + X_T R}{1 + R} \quad (7)$$

where  $X_0 = \frac{X_T F_2}{F_1 + F_2}$  is the mean coordinate of the photocenter of the double system in the absence of a transient event. The parameters  $X_C$  and  $R$  are GAIA observables from which we can estimate the distance between the objects and reconstruct the light curve of the transient event.

#### *The case with a quasi-stationary object and a visible linear motion of an variable brightness object.*

Similar cases take place with blazars, which demonstrate the presence of strong optical jets directed toward the observer at a small angle. In the calculation of the distribution  $(\mu, \epsilon)$ , the coordinate  $X_T$ , in contrast to the previous case, varies linearly with time:  $X_T = X_{T0} + \mu_{jet} t$ , where  $X_{T0}$  is the coordinate of TE at the initial moment of the GAIA catalog. Then, by the formula (4) the apparent proper motion measured by Gaia is calculated as:  $\mu = \frac{R}{(R+1)} \mu_{jet} + o(\xi')$ . And  $o$ -small is the linear part of the random parameter  $\xi'$ , which includes the relative variability of the jet in addition to the relative variability of the core. The  $\epsilon$  is a function of the ratio of TE to AGN fluxes ( $R$ ), the relative internal variability of AGN and jet ( $\xi'$ ), the TE coordinate at the initial time of the GAIA catalog ( $X_{T0}$ ), and the apparent proper motion of TE ( $\mu_{jet}$ ). The calculation of this parameter is beyond the scope of this study.

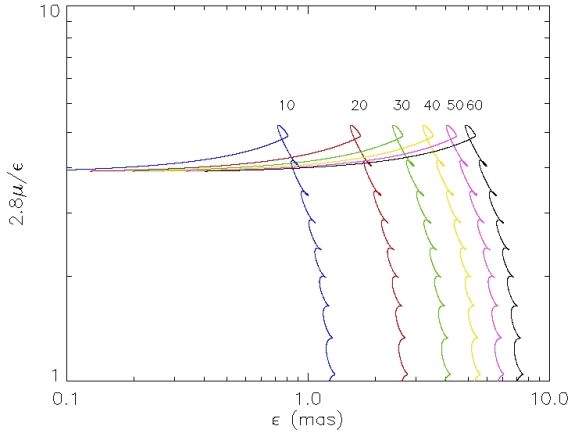


**Fig. 6.** Variation of the model curves as a function of the distance of the transient from the nucleus  $X_T$  ( $R_0 = 1, \alpha = 110^d, \sigma = 10^d$ ). The numbers indicate the values of these distances in *mas* units.

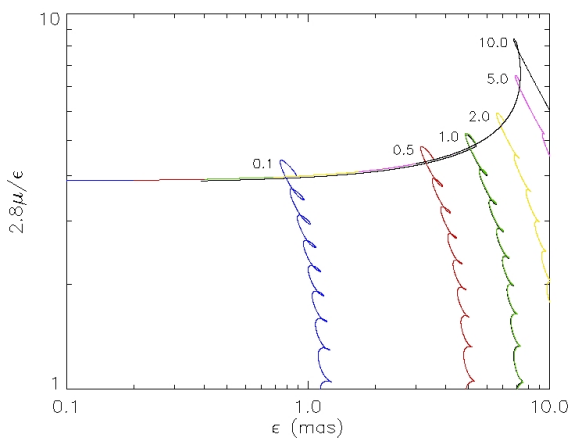


**Fig. 7.** Variation of the model curves as a function of the ratio of the fluxes of the transient event to the flux from the AGN at time  $t_{peak}$ ,  $R_0$  ( $X_T = 60$  mas,  $\alpha = 110^d, \sigma = 10^d$ ). The numbers indicate the values of  $R_0$  corresponding to the curves.

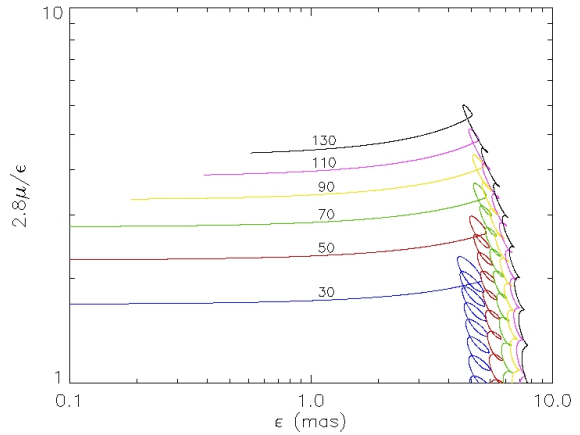


**Fig. 8.** Variation of model curves depending on the exponential decay parameter  $\alpha$  ( $R_0 = 1, X_T = 60$  mas,  $\sigma = 10^d$ ). The numbers indicate the values of these parameters in days.

Table 1: Catalog.

SRG e+	GAIa EDR3+	RA	DEC	$\mu$ (mas/yr)	z	Type	Simbad	Reference
J000310.1+044455	2741905339356533504	00 03 10.02	+04 44 56.2	1.94 ± 0.51	0.058	Sy2	2MASXJ00030999+0444564	2003A&A...412...45P
J001124.6+380935	287777175068230176	00 11 24.46	+38 09 33.7	5.72 ± 1.48	0.137	AGN	None	2022AstL...48..724K
J002848.8+145216	2780286129184910208	00 28 48.78	+14 52 16.3	3.29 ± 0.77	0.089	Sy1	2MASXJ00284876+1452156	2012ApJS...203...21A
J002936.8-173833	2367248023501811840	00 29 36.79	-17 38 30.4	3.85 ± 0.30	0.054	Galaxy	2MASXJ00293678-1738306	2009MNRAS.399..683J
J003246.0-193831	236344227016064480	00 32 46.03	-19 39 30.4	3.12 ± 0.85	0.054	Galaxy	2MASXJ00324605-1938303	2009MNRAS.399..683J
J003415.5-274813	231932144551836928	00 34 15.47	-27 48 12.7	3.69 ± 0.44	0.005	Galaxy SF	NGC150	2012ApJS...203...21A
J003826.9-000039	2543475415864489472	00 38 26.67	-00 00 42.7	2.99 ± 0.68	0.045	Galaxy	MCG+00-02-101	2012ApJS...203...21A
J004447.5+152910	2781106124341566976	00 44 47.34	+15 29 11.9	6.51 ± 1.17	0.227	Sy1	SDSSJ004447-33+152911.8	2012ApJS...203...21A
J005055.9+283325	311984160934363392	00 50 55.69	+29 33 28.1	4.56 ± 0.71	0.136	QSO	2MASSJ00505570+2933281	2011MNRAS.414..500H
J010812.2+845152	5738811985223210368	01 08 11.86	+85 41 50.7	3.35 ± 0.60	0.077	Sy2	None	2022AstL...48..724K
J010816.3-113401	2469702471186911616	01 08 16.31	-11 34 01.0	2.85 ± 0.58	0.047	Galaxy	2MFGC829	2009MNRAS.399..683J
J011014.2+501030	403565954748186496	01 10 14.06	+50 10 31.0	2.81 ± 0.65	0.024	Sy	2MASXJ01101406+5010313	2003A&A...412...45P
J011711.2-220903	235162334479528544	01 17 11.23	-22 09 03.6	1.52 ± 0.32	0.090	Galaxy	2MASXJ01171123-2209037	2009MNRAS.399..683J
J011959.3+144712	2591270390924029056	01 19 59.60	+14 47 10.4	4.83 ± 0.52	0.014	Galaxy R	NGC471	2018ApJ...861..49H
J012048.0-082918	2472133530051650048	01 20 48.01	-08 29 18.4	4.10 ± 0.71	0.034	AGN	MCG-02-04-026	2005PASA...22..277J
J012531.6+320811	31643474385650560	01 25 31.46	+32 08 10.5	1.62 ± 0.40	0.016	Sy2	Mrk933	2018ApJ...861..49H
J013435.8+022837	2558952819311344256	01 34 35.91	+02 28 39.9	3.51 ± 0.68	0.177	QSO	2MASSJ01343589+0228397	2018A&A...613A..51P
J014238.5-054140	2480153505303646080	01 42 38.57	-04 51 41.1	2.98 ± 0.65	0.040	Galaxy	2MASXJ01423859-0451414	2003AJ...126.21252R
J014417.5+314004	303683913296921728	01 44 17.27	+31 40 03.3	9.32 ± 1.93	0.124	QSO	SDSSJ014417-27+314003.3	2020ApJS...250...8L
J014458.6-023200	2505449660085548576	01 44 58.56	-02 31 59.0	1.98 ± 0.24	0.096	Galaxy	2MASXJ01445853-0231589	2009MNRAS.399..683J
J014916.6+851529	57379873587070032	01 49 18.04	+85 15 37.2	4.15 ± 1.10	0.004	Galaxy	UGC1198	2003A&A...412...45P
J020436.8-115942	5151365323643149568	02 04 36.76	-11 59 43.4	1.76 ± 0.29	0.073	Sy1	2MASXJ02043675-1159432	2009MNRAS.399..683J
J021049.7+240709	104299409979045376	02 10 49.38	+24 07 06.7	2.71 ± 0.60	0.144	Sy1	None	2022AstL...48..724K
J021257.5+140609	77274609208701824	02 12 57.60	+14 06 10.2	3.66 ± 0.41	0.062	Sy1	2MASXJ02125762+1406105	2012ApJS...203...21A
J022534.1+264400	103529675570132992	02 25 33.77	+26 44 01.7	4.86 ± 0.66	0.035	Galaxy	UGC1881A	2018MNRAS.474.1873W
J023800.0+193812	878223358125418112	02 37 59.99	+19 38 11.8	1.68 ± 0.44	0.034	Galaxy	LEDA1599918	2018ApJ...861..49H
J024012.2-023344	2495867038292425280	02 40 12.22	-02 33 44.4	2.73 ± 0.39	0.043	Galaxy	2MASXJ02401221-0233438	2009MNRAS.399..683J
J024443.5+204136	85364953204844416	02 44 43.31	+20 41 38.6	1.79 ± 0.46	0.051	Sy2	None	2022AstL...48..724K
J032006.4+402200	2362653993361163328	03 20 06.32	+40 21 58.7	2.55 ± 0.62	0.047	Sy1	2MASXJ03200634+4021583	2020ApJS...249...3A
J032513.1+404154	236149950616287360	03 25 12.95	+40 41 52.8	3.45 ± 0.75	0.047	Sy2	LEDA97012	2020A&A...640A..30M
J040550.9+843716	56971961215506208	04 05 51.36	+81 37 17.2	1.97 ± 0.41	0.118	Sy1	None	2022AstL...48..724K
J043122.0+605458	472342743530601984	04 31 22.51	+60 55 00.2	7.50 ± 0.79	0.015	Galaxy	2MASXJ04312250+6055002	2011MNRAS.416.2840L
J044110.7+683728	495873426235161344	04 41 11.00	+68 37 29.3	3.87 ± 0.66	0.120	AGN	None	2022AstL...48..724K
J050808.7+700529	497736754846822656	05 08 09.16	+70 05 30.1	5.93 ± 0.63	0.028	Galaxy	2MASXJ05080919+7005304	2000MNRAS.317..55S
J051316.6+632751	482638261175017216	05 13 16.43	+66 27 50.2	5.12 ± 0.94	0.015	Galaxy	2MASXJ05131637+6627498	1999PASP..111..438F
J053532.1+401116	191175111110250752	05 35 32.13	+40 11 15.8	1.15 ± 0.23	0.021	Sy1	LEDA2161985	2014A&A...561A..67P
J053821.8+733515	553597546173225216	05 38 23.46	+79 35 12.7	4.27 ± 0.60	0.015	AGN	None	1999PASP..111..438F <sup>2</sup>
J062329.3+691238	1106940173151909888	06 23 29.08	+69 12 32.6	4.54 ± 0.92	0.055	AGN	None	2022AstL...48..724K
J063147.1+655440	11042301518641373888	06 31 47.43	+65 54 42.5	1.97 ± 0.44	0.108	AGN	None	2022AstL...48..724K
J063709.8+55349	9942751039680768	06 37 09.94	+53 53 46.1	3.41 ± 0.50	0.034	Galaxy	2MASXJ06370993+5353466	1999MNRAS.308..897L
J065236.7+454651	954117334016424064	06 52 36.99	+45 46 50.2	4.90 ± 0.78	0.021	Sy2	MCG+08-13-022	2002LEDA.....0P
J070634.5+635057	1099887149653797120	07 06 34.82	+63 50 56.1	2.58 ± 0.27	0.014	Galaxy	UGC3660	2003A&A...412..45P

<sup>2</sup>Spectroscopic observations were carried out on the RTT-150, 2022AstL...48..724K

Continuation of the table 1

SRG e+	GAIa EDR3+	RA	DEC	$\mu$	z	Type	Simbad	Reference
J072528.5+434332	973218805928899584	07 25 28.48	+43 43 32.3	3.52 ± 0.91	0.069	Sy1	2MASXJ072528851+4343319	2012ApJS..203...21A
J072546.6+531200	986865806813601408	07 25 46.68	+53 11 59.1	0.94 ± 0.20	0.039	Galaxy	2MASXJ07254669+5311598	2000AJ....120.2338R
J074008.9+800356	11422233981003897984	07 40 08.90	+80 03 57.1	1.91 ± 0.34	0.087	Sy1	2E1829	1991ApJS..76..813S
J075244.3+455658	92658233041407616	07 52 44.21	+45 56 57.4	1.29 ± 0.34	0.052	BLL	2MASXJ07524421+4556576	2012ApJS..203...21A
J080435.2+504231	93504242181701248	08 04 35.51	+50 42 30.7	3.71 ± 0.87	0.023	AGN	2MASXJ08043556+5042305	2015ApJS..219...12A
J090436.8+533603	1035985561071454080	09 04 36.95	+55 36 02.7	1.57 ± 0.15	0.037	Sy1	2MASXJ09043699+5536025	2012ApJS..203...21A
J090554.9+471046	1012216456141389440	09 05 54.50	+47 10 45.5	4.08 ± 0.77	0.027	LINER	UGC4765	2012ApJS..203...21A
J091118.8+462311	1011377902430454016	09 11 18.96	+46 23 07.2	7.93 ± 0.99	0.103	LINER	2MASXJ09111899+4623069	2012ApJS..203...21A
J092108.6+454542	818703921480587904	09 21 08.59	+44 54 50.8	1.66 ± 0.36	0.156	Sy1	2MASXJ09210857+4454507	2012ApJS..203...21A
J095033.0+441850	820500351682252544	09 50 33.15	+44 18 51.6	1.76 ± 0.35	0.016	AGN	NGC3010	2012ApJS..203...21A
J101148.0+504959	8480927334119805696	10 11 48.35	+50 50 00.5	2.62 ± 0.70	0.079	Sy1	2MASXJ10114829+5050007	1995MNRAS.277.1312C
J101653.5+732404	1078032981660206080	10 16 53.65	+73 24 02.7	3.44 ± 0.73	0.009	Sy2	NGC3147	2003A&A..412...45P
J101739.0+420059	805227344901870592	10 17 38.72	+42 01 03.3	3.94 ± 0.32	0.107	Sy1	2MASXJ10173874+4201035	2009ApJS..182..543A
J102233.8+582706	104719130746301824	10 22 33.70	+58 27 04.9	1.33 ± 0.32	0.077	Sy1	2MASXJ10223371+5827044	2012ApJS..203...21A
J104118.9+574501	8543811974290712960	10 41 19.22	+57 45 00.1	1.13 ± 0.28	0.068	Sy2	2MASXJ10411919+5745000	2012ApJS..203...21A
J105057.2+533213	86139005524754800	10 50 57.29	+59 32 14.5	1.41 ± 0.19	0.085	Sy1	2MASXJ10505729+5932144	2012ApJS..203...21A
J105946.4+455409	783159424976854784	10 59 46.68	+45 54 09.7	1.39 ± 0.31	0.179	AGN	2MASXJ10594667+4554098	2012ApJS..203...21A
J110241.8+420655	77825264817597920	11 02 41.47	+42 06 51.9	7.02 ± 0.90	0.075	Sy1	2MASXJ11024141+4206516	2012ApJS..203...21A
J110503.8+505951	839151745380126336	11 05 04.21	+50 59 49.9	9.43 ± 1.30	0.118	Sy1	LEDA2386530	2016ApJ...818..113N
J110647.5+723407	1075615563616899328	11 06 47.46	+72 34 07.3	1.57 ± 0.17	0.009	Sy1	NGC316	2001AJ...121.2843B
J1110919.8+714233	1075317668976301504	11 09 19.75	+71 42 33.4	1.20 ± 0.25	0.130	Sy1	RXJ1109.2+7142	2012ApJS..203...21A
J111705.3+470212	78857682185589624	11 17 05.21	+47 02 14.3	3.38 ± 0.56	0.188	Sy1	2MASXJ11170521+4702148	2012ApJS..203...21A
J112218.0+590430	85762096374678032	11 22 17.90	+59 04 28.3	1.88 ± 0.43	0.005	LINER	NGC3642	2016A&A..595A..118V
J112348.0+465649	78871326006877048	11 23 48.04	+46 56 50.1	2.08 ± 0.46	0.157	Sy1	2MASXJ11234805+4656501	2012ApJS..203...21A
J112958.2+462100	785529662805821312	11 29 57.95	+46 20 59.5	1.29 ± 0.33	0.210	Sy1	LAMOSTJ112957.96+462059.5	2012ApJS..203...21A
J113234.9+530404	841054411602049280	11 32 34.85	+53 04 45.5	3.01 ± 0.61	0.003	Galaxy	NGC3718	2017ApJ...850...74K
J113925.5+451345	773886418783213312	11 39 25.56	+45 13 46.7	3.38 ± 0.51	0.127	Sy1	2MASXJ11392557+4513464	2012ApJS..203...21A
J114432.7+613157	85991698454364688	11 44 33.06	+61 32 00.7	1.41 ± 0.29	0.048	Sy1	MCG+10-17-057	2012ApJS..203...21A
J114958.1+575108	845401781789519872	11 49 58.09	+57 51 07.7	1.06 ± 0.28	0.100	Sy1	2MASXJ11495809+5751081	2012ApJS..203...21A
J115107.2+50441	841656192350581376	11 51 06.87	+55 04 43.4	3.85 ± 0.90	0.020	Galaxy	NGC3921	2003A&A..412...45P
J120215.3+40321	1537913095891025152	12 02 15.46	+44 03 19.7	3.80 ± 0.72	0.101	LINER	2MASXJ12021545+4403194	2009ApJS..182..543A
J120655.4+501736	154670211510764160	12 06 55.63	+50 17 37.2	3.03 ± 0.48	0.061	Sy1	MCG+08-22-071	2012ApJS..203...21A
J121049.6+328281	15355810559076616192	12 10 49.61	+39 28 22.1	3.54 ± 0.62	0.022	LINER	NGC4156	2012ApJS..203...21A
J121607.1+504930	154752767653872288	12 16 07.10	+50 49 30.1	0.67 ± 0.17	0.031	Sy1	Mrk1469	2012ApJS..203...21A
J121651.9+375437	153238492225589120	12 16 51.77	+37 54 38.1	3.50 ± 0.46	0.063	Sy2	2E2635	2012ApJS..203...21A
J121745.9+534902	157228830437823616	12 17 45.79	+53 49 02.4	2.02 ± 0.49	0.194	Sy1	2MASXJ12174579+5349023	2012ApJS..203...21A
J123152.1+450442	154158471310931744	12 31 52.05	+45 04 43.1	1.29 ± 0.16	0.062	Sy1	2MASXJ12315204+4504428	2012ApJS..203...21A
J123429.8+621808	1583600827682206080	12 34 29.86	+62 18 06.2	0.84 ± 0.22	0.135	Sy1	LEDA3096159	2012ApJS..203...21A
J123503.3+622336	1680638849162446592	12 35 02.66	+66 22 33.5	5.41 ± 0.75	0.047	Galaxy SF	Mrk217	2009ApJS..182..543A
J123553.8+421117	153454649366340992	12 35 53.51	+42 41 21.0	4.44 ± 0.92	0.155	Sy1	2MASXJ12355351+4241207	2009ApJS..182..543A
J123740.2+611148	1580153004031345920	12 37 40.72	+61 11 48.6	4.10 ± 0.67	0.181	Sy1	2MASXJ12374071+6111483	2012ApJS..203...21A
J124235.8+780719	1717177201102073856	12 42 36.10	+78 07 20.4	4.30 ± 0.74	0.022	Sy1	LEDA140000	1996ApJS..106..341M
J124310.7+731600	168988970452126080	12 43 11.22	+73 15 59.3	4.96 ± 0.76	0.075	Galaxy R	NVSSJ124310.7+731600	2002MNRAS.329.700S
J124412.0+504201	156778930501508352	12 44 12.06	+50 42 02.0	1.67 ± 0.41	0.216	Sy1	2MASXJ12441206+5042020	2012ApJS..203...21A
J124441.5+374023	1520417980403049728	12 44 41.48	+37 40 25.1	3.24 ± 0.87	0.166	Sy1	2MASXJ12444144+3740249	2012ApJS..203...21A

Continuation of the table 1

SRCe+	RA	DEC	$\mu$ (mas/yr)	$\mu$	$\nu$	Type	Simbad	Reference
J124612.1+410813	15224139094057902464	12 46 12.11	+41 08 11.9	0.73 ± 0.15	0.067	Sy1	LEDA140004	2012ApJS..203...21A
J124617.4+282033	3962816210617909760	12 46 17.34	+28 20 33.9	5.35 ± 0.85	0.100	Sy2	2MASXJ12461737+2820343	2009ApJS..182..543A
J130041.0+523217	155803660251731360	13 00 40.78	+52 32 15.8	4.20 ± 0.86	0.054	Galaxy SF	2MASXJ13004073+5232155	2012ApJS..203...21A
J130301.0+403840	1527295150757420160	13 03 01.05	+40 38 40.6	1.23 ± 0.29	0.067	Sy1	2MASXJ13030101+4038401	2012ApJS..203...21A
J130422.3+361542	1516302989417314144	13 04 22.19	+36 15 43.2	2.31 ± 0.45	0.045	Sy2	2MASXJ13042219+3615428	2012ApJS..203...21A
J130702.9+563155	1564940504747175296	13 07 02.89	+56 31 58.4	3.09 ± 0.46	0.081	Sy1	MCG+10-19-053	2012ApJS..203...21A
J131056.2+444412	1529712564510717696	13 10 56.19	+44 44 13.6	0.92 ± 0.20	0.060	Sy1	[VV2006c]J131056.2+444413	2012ApJS..203...21A
J131118.5+463502	15539881663345499136	13 11 18.54	+46 35 02.3	14.94 ± 0.84	0.271	QSO	2MASSJ13111853+4635024	2009ApJS..182..543A
J131447.1+290624	1447726002515875712	13 14 47.07	+26 06 24.1	3.21 ± 0.29	0.072	Sy1	2MASXJ13144704+2606244	2012ApJS..203...21A
J131517.4+442422	1526644239872942592	13 15 17.26	+44 24 25.5	5.33 ± 1.46	0.035	Sy2	Mrk248	2012ApJS..203...21A
J132024.6+690011	1684884819471591552	13 20 24.61	+69 00 11.6	0.61 ± 0.14	0.067	Sy1	LEDA2726469	1993AJ...105..2079R
J132038.0+341128	1472901554617233664	13 20 37.89	+34 11 26.2	2.44 ± 0.32	0.064	AGN	2MASXJ13203789+3411258	2002ApJ...123..3018M
J132811.7+622745	1663791754044480384	13 28 11.58	+62 27 43.0	2.33 ± 0.48	0.091	Sy2	2MASSJ13281159+6227431	2009ApJS..182..543A
J132946.5+553618	1565167485177736448	13 29 45.92	+55 36 13.4	1.35 ± 0.28	0.017	Galaxy SF	Mrk257	2012ApJS..203...21A
J133106.6+510929	1559600967046402048	13 31 06.88	+51 09 30.9	6.85 ± 1.26	0.179	Sy1	2MASSJ13310685+5109309	2012ApJS..203...21A
J133147.1+591048	1662178495608598656	13 31 47.08	+59 10 47.2	2.01 ± 0.42	0.043	Sy2	MCG+10-19-053	2012ApJS..203...21A
J133651.1+365018	1472091004093186432	13 36 50.95	+36 50 18.0	5.15 ± 0.76	0.062	Galaxy SF	2MASXJ13365093+3650182	2012ApJS..203...21A
J133804.5+394110	1499986305580569216	13 38 04.30	+39 41 10.1	2.16 ± 0.41	0.060	Sy2	2MASSJ13380430+3941102	2009ApJS..182..543A
J133826.9+321254	1468887892260813660	13 38 26.87	+32 12 52.7	1.95 ± 0.35	0.089	Sy1	2MASXJ13382685+3212524	2012ApJS..203...21A
J134208.5+333915	14713609670285696	13 42 08.38	+35 39 15.5	0.32 ± 0.06	0.003	Sy1	NGC5273	2017ApJ...850...74K
J134220.2+384210	1496694299048016512	13 42 20.15	+38 42 09.7	3.02 ± 0.36	0.079	Sy1	2MASXJ13422018+3842096	2012ApJS..203...21A
J134330.0+510204	155894005747825136	13 43 30.01	+51 02 04.1	2.93 ± 0.66	0.131	LINER	2MASSJ13433000+5102041	2009ApJS..182..543A
J134353.3+803549	1718748746815817472	13 43 52.89	+80 35 49.4	2.46 ± 0.46	0.045	AGN	2MASXJ13435300+8035495	1999PASP..111..438F
J134448.7+394420	1455742610513541376	13 44 48.63	+30 44 20.4	2.86 ± 0.48	0.077	Sy1	2MASXJ13444864+3044204	2020ApJS..249...3A
J134834.9+263110	14513274787212475776	13 48 34.95	+26 31 09.9	3.31 ± 0.38	0.059	Sy2	2E3140	2012ApJS..203...21A
J134915.1+220034	12510981340977479232	13 49 15.20	+22 00 32.6	0.86 ± 0.17	0.062	Sy1	LEDAA661730	2020ApJS..249...3A
J135317.5+322929	1458659683583166336	13 53 17.80	+33 29 27.0	2.01 ± 0.42	0.008	Sy2	NGC5347	2018ApJ...861..49H
J135420.0+325549	145758507088809856	13 54 19.95	+32 55 47.7	1.50 ± 0.41	0.026	Sy2	Mrk633	2015ApJS..219...12A
J135620.6+264356	1450823498570440832	13 56 20.70	+26 43 54.4	8.86 ± 1.54	0.062	Sy1	LEDA1786612	2012ApJS..203...21A
J135830.7+200546	1246851481593437440	13 58 30.78	+20 05 51.2	2.84 ± 0.72	0.062	Sy1	2MASXJ13583078+2005515	2009ApJS..182..543A
J140517.8+174910	1245314329978856960	14 05 18.07	+17 49 14.4	3.26 ± 0.73	0.104	Sy1	LEDA1542593	2012ApJS..203...21A
J140845.5+333219	148257282453594624	14 08 45.73	+35 32 18.6	3.60 ± 0.64	0.166	Sy2	2MASXJ14084576+3532186	2012ApJS..203...21A
J141109.3+444012	150475416595674562	14 11 09.17	+44 40 11.9	4.29 ± 1.09	0.095	Sy1	2MASSJ14110916+4440119	2012ApJS..203...21A
J141222.9+335716	1479178151105353216	14 12 22.83	+33 57 15.5	3.36 ± 0.78	0.116	Galaxy SF	2MASXJ14122281+3357152	2012ApJS..203...21A
J141238.3+391836	1485338744822384384	14 12 38.15	+39 18 36.8	3.62 ± 0.42	0.026	Sy1	NGC515	2012ApJS..203...21A
J141415.3+264449	12592662048821618816	14 14 15.18	+26 44 51.4	1.06 ± 0.19	0.035	Sy2	Mrk670	2012ApJS..203...21A
J141607.9+32036	14794099725799872	14 16 07.75	+35 20 37.8	6.75 ± 1.06	0.013	Sy2	NGC533	2018ApJ...861...49H
J141942.9+491412	1508267002527518464	14 19 43.23	+49 14 11.9	6.10 ± 0.64	0.026	AGN	Mrk1490	2012ApJS..203...21A
J142307.8+283541	128388943091824000	14 23 07.51	+28 35 42.3	4.25 ± 0.65	0.029	Sy2	2MASXJ14230749+2835418	2015ApJS..219...12A
J142630.7+390345	1490705907750159104	14 26 30.68	+39 03 43.4	0.51 ± 0.10	0.081	Sy1	LEDA3093357	2012ApJS..203...21A
J142808.1+464203	150664078302144800	14 28 08.10	+46 42 03.3	3.04 ± 0.39	0.074	Sy1	2MASXJ14280814+4642037	2012ApJS..203...21A
J142817.8+571015	1610593773720675584	14 28 17.99	+57 10 18.5	2.05 ± 0.21	0.043	Sy2	2MASXJ14281793+5710187	2009ApJS..182..543A
J143016.1+230345	1254429624969681664	14 30 16.04	+23 03 44.5	3.05 ± 0.58	0.081	Sy2	2MASXJ14301603+2303445	2012ApJS..203...21A
J143318.3+344404	1480032677798584960	14 33 18.48	+34 44 04.4	3.06 ± 0.65	0.034	LINER	UGC9367	2017ApJS..233..25A
J143452.5+483943	160329864721395808	14 34 52.46	+48 39 42.7	0.68 ± 0.14	0.037	Sy1	NGC5683	2017ApJS..233..25A

Continuation of the table 1

SRGe+	GAIA EDR3+	RA	DEC	$\mu$ (mas/yr)	$\nu$ (mas/yr)	$z$	Type	Simbad	Reference
J143701.5+264019	1279530852661016576	14 37 01.50	+26 40 19.2	2.08 ± 0.40	0.218	QSO	2MASXJ14370150+2640191	2012ApJS..203...21A	
J143731.8+155549	123441555840658752	14 37 31.70	+15 55 47.6	3.64 ± 0.45	0.037	Sy1	2MASXJ14373169+1555479	2015ApJS..219...12A	
J143820.9+464940	1494885568060805376	14 38 21.17	+46 49 43.7	4.02 ± 1.07	0.324	AGN	SDSSJ143821.16+464943.7	2015ApJS..219...12A	
J143936.3+455504	14938412028446433152	14 39 36.35	+44 55 04.3	6.03 ± 0.66	0.088	Sy1	2MASXJ14393635+4455042	2012ApJS..203...21A	
J144026.2+332703	128676244801626112	14 40 25.84	+33 27 02.6	9.41 ± 2.24	0.275	Sy1	SDSSJ144025.84+332702.5	2012ApJS..203...21A	
J144214.4+291808	128248421390548992	14 42 14.63	+29 18 08.9	3.78 ± 0.83	0.062	Galaxy SF	2MASXJ14421460+2918093	2012ApJS..203...21A	
J144227.5+555848	1607566096654997760	14 42 27.61	+55 58 46.4	4.61 ± 0.33	0.077	Galaxy SF	2MASXJ14422754+5558465	2012ApJS..203...21A	
J144331.4+492335	15911767832551398400	14 43 31.26	+49 23 35.2	5.82 ± 1.34	0.030	AGN	2MASXJ14433125+4923353	2009ApJS..182..543A	
J144640.4+162402	1186652842015404416	14 46 40.21	+16 24 02.2	2.31 ± 0.27	0.054	Sy1	2MASXJ14464020+1624021	2012ApJS..203...21A	
J144738.9+610655	1617866390303368192	14 47 39.33	+61 06 56.0	1.37 ± 0.30	0.137	Sy1	LEDA2816925	2012ApJS..203...21A	
J144819.4+443232	149066983321127936	14 48 19.38	+44 32 32.7	4.80 ± 0.72	0.080	Sy1	LEDA2246593	2012ApJS..203...21A	
J144924.5+321815	1283349981906069568	14 49 24.44	+32 18 16.2	3.29 ± 0.27	0.058	QSO	LEDA1990685	2018AJ...155..189D	
J145229.7+383425	129624535802396800	14 52 29.63	+38 34 24.7	3.76 ± 0.88	0.068	Sy1	2MASXJ14522965+3834251	2009ApJS..182..543A	
J145404.9+363317	1293628417091927552	14 54 04.58	+36 33 20.5	5.20 ± 1.14	0.071	Galaxy SF	2MASXJ14540453+3633207	2012ApJS..203...21A	
J145425.5+464525	159033650892983200	14 54 25.48	+46 45 24.1	8.99 ± 0.81	0.069	Sy1	2MASXJ14542548+4645239	2012ApJS..203...21A	
J145517.7+173831	11883065576223165696	14 55 17.69	+17 38 29.7	2.41 ± 0.62	0.095	Sy1	2MASXJ14551769+1738297	2012ApJS..203...21A	
J150843.0+281018	1274804400069294976	15 08 42.62	+28 10 16.2	3.65 ± 0.78	0.026	Galaxy SF	LEDA84441	2017AJ...154..86W	
J150852.9+681407	1693563917585165440	15 08 52.81	+68 14 07.0	0.68 ± 0.13	0.058	Sy1	2MASXJ15085291+6814074	2016ApJ...818..113N	
J150909.0+000222	1166949486271776640	15 09 08.76	+09 02 21.0	2.65 ± 0.36	0.044	QSO	ZTF-21	2017A&A..597A..79P	
J151345.7+311129	1276379519191952896	15 13 45.76	+31 11 25.1	7.37 ± 1.41	0.072	Galaxy SF	2MASXJ15134575+3111250	2012ApJS..203...21A	
J151444.8+265431	127143331777425792	15 14 44.82	+26 54 32.5	5.12 ± 0.64	0.138	Galaxy SF	SDSSJ151444.81+265432.4	2012ApJS..203...21A	
J151721.7+465812	1588105221880335584	15 17 22.00	+46 58 12.9	17.63 ± 2.3	0.154	Galaxy SF	None	Current paper	
J151751.7+050628	1156171390396557056	15 17 51.71	+05 06 27.8	4.22 ± 0.49	0.039	Sy1	2MASXJ15175169+0506278	2012ApJS..203...21A	
J152043.3+301423	1276861924992024768	15 20 43.23	+30 41 22.6	0.65 ± 0.11	0.077	Sy1	2MASXJ15204320+3041228	2012ApJS..203...21A	
J152240.1+310858	127690347084532064	15 22 40.24	+31 08 56.7	4.32 ± 0.71	0.116	Galaxy R	FIRSTJ152240.2+310856	1998AJ...116..1529H	
J152345.3+322820	12773110324506209280	15 23 45.08	+32 28 22.4	2.88 ± 0.62	0.077	Sy1	2MASXJ15234513+3228222	2000AN...321...1S	
J152433.4+274311	1270990984505904640	15 24 33.35	+27 43 11.6	5.30 ± 0.52	0.069	Sy1	2MASXJ15243338+2743117	2016ApJ...832..67N	
J153333.1+321813	1274488977669512192	15 33 33.16	+32 18 13.5	3.68 ± 0.74	0.065	Sy1	2MASXJ15333315+3218134	2009ApJS..182..543A	
J153344.4+235815	1220979801197880448	15 33 44.60	+23 58 11.9	4.20 ± 0.41	0.067	Sy1	2MASXJ15334460+2358119	2009ApJS..182..543A	
J153937.1+591954	1602979758777666432	15 39 37.06	+59 19 55.2	4.13 ± 0.97	0.008	Sy	NGC5985	2003A&A..412..45P	
J154450.1+440742	1396627982025903616	15 44 50.38	+44 07 43.6	3.60 ± 0.75	0.255	Sy1	2MASXJ15445037+4407436	2005ApJ...130..367S	
J154529.6+251128	1222781282277296256	15 45 29.63	+25 11 27.9	2.82 ± 0.59	0.117	Sy2	2MASXJ15452960+2511283	2012ApJS..203...21A	
J155340.4+434405	1396689902570254208	15 53 40.36	+43 44 04.9	4.06 ± 0.96	0.040	LINER	2MASXJ15534030+4344046	2002AJ...124..3405S	
J155640.4+451339	1396931107932365920	15 56 40.32	+45 13 38.4	3.09 ± 0.65	0.181	Sy2	SDSSJ155640.32+451338.4	2015ApJS..219...12A	
J155943.9+274232	1316581065919736576	15 59 43.94	+27 42 29.7	3.04 ± 0.79	0.051	Galaxy SF	2MASXJ15594391+2742299	2012ApJS..203...21A	
J160508.8+323922	1323103506333569280	16 05 08.88	+32 39 21.5	1.48 ± 0.40	0.091	Sy1	LEDA2006774	2015ApJS..219...12A	
J160851.4+257119	131878919450704192	16 08 51.07	+29 57 15.0	9.98 ± 1.51	0.048	Sy1	2MASXJ16085109+2957144	2012ApJS..203...21A	
J161159.6+311043	132198499377093808	16 11 59.55	+31 10 41.5	3.23 ± 0.63	0.159	Sy1	LEDA1935181	2009ApJS..182..543A	
J161318.4+361617	1330140288953474816	16 13 18.50	+36 16 21.9	7.71 ± 1.23	0.082	LINER	SDSSJ161318.51+361621.8	2012ApJS..203...21A	
J161456.2+413058	1381645559845677184	16 14 56.18	+41 30 55.8	2.18 ± 0.52	0.196	Sy1	2MASXJ16145620+4130560	2015ApJS..219...12A	
J161818.6+421914	138211347076273584	16 18 18.49	+42 19 14.2	2.84 ± 0.49	0.165	Sy1	2MASXJ16181850+4219141	2012ApJS..203...21A	
J161944.9+243432	130247515636900748	16 19 44.98	+24 34 31.9	1.69 ± 0.22	0.065	Sy1	2MASXJ16194498+2434318	2015ApJS..219...12A	
J162052.6+540058	1428334190814957056	16 20 52.60	+54 00 58.6	1.54 ± 0.34	0.146	Sy1	2MASXJ16205259+5400587	2009ApJS..182..543A	
J162315.2+322825	132876853383878624	16 23 15.16	+34 28 24.1	3.96 ± 1.07	0.165	Sy1	2MASXJ16231516+3228239	2009ApJS..182..543A	
J162433.5+555456	1429521044897260544	16 24 33.47	+55 54 52.6	5.73 ± 0.86	0.031	Galaxy	2MASXJ16243340+5554521	1999PASP..111..438F	

Continuation of the table 1

SRG+e+	RA	DEC	$\mu$ (mas/yr)	$\mu$	$\nu$	$\zeta$	Type	Simbad	Reference
J162501.5+241546	13022119554275260032	16 25 01.44	+24 15 47.4	1.70 ± 0.33	0.050	Sy1	2MASXJ16250142+2415473	2012ApJS..203...21A	
J162921.9+413357	1333056354308113664	16 29 21.83	+41 33 55.5	3.58 ± 0.78	0.161	Sy1	2MASXJ16292185+4133553	2012ApJS..203...21A	
J162948.2+672242	1648419928654134784	16 29 48.38	+67 22 42.0	1.14 ± 0.25	0.025	Sy1	Mrk85	1992&AS..93..211F	
J163202.6+320338	132426514898399104	16 32 02.48	+32 03 39.4	1.53 ± 0.26	0.059	Sy1	2MASXJ16320244+3203397	2015ApJS..219...12A	
J163221.1+641052	1629118483063501696	16 32 20.70	+64 10 53.5	5.31 ± 0.84	0.065	Galaxy	2MASXJ16322060+6410539	1999MNRAS.308..897L	
J163508.8+461248	140711499078539264	16 35 09.19	+46 12 50.1	3.65 ± 0.92	0.031	Galaxy	IC1222	2017AJ....154..86W	
J164058.9+114405	444729017087901280	16 40 58.89	+11 44 04.2	2.05 ± 0.32	0.078	BLL	LEDA58746	2011ApJ...741...30A	
J164313.8+055416	4446025560705328656	16 43 13.78	+09 54 16.2	1.63 ± 0.17	0.047	Galaxy	2MASXJ16431379+0954163	1999PASP..111..438F	
J164819.0+302211	1311567877011972608	16 48 19.02	+30 22 10.8	1.48 ± 0.34	0.102	Sy1	LEDA1901045	2009ApJS..182..543A	
J164903.7+190306	45632867946970127616	16 49 03.65	+19 03 07.1	3.05 ± 0.56	0.148	Sy1	SDSSJ164903.65+190307.1	2012ApJS..203...21A	
J165121.8+215530	4565704377731941632	16 51 21.88	+21 55 26.3	2.01 ± 0.45	0.055	Sy2	2MASXJ16512188+2155264	2012ApJS..203...21A	
J165129.6+192502	45622898527137478656	16 51 29.52	+19 24 59.9	3.61 ± 0.93	0.023	LINER	UGC10585	2015ApJS..219...12A	
J165251.5+172650	4559362016706811176	16 52 51.42	+17 26 51.0	5.68 ± 0.59	0.034	Galaxy	2MASXJ16525143+1726514	1999PASP..111..438F	
J165315.4+234941	4566562099880989696	16 53 15.06	+23 49 42.9	8.61 ± 1.05	0.103	Sy2	IRAS16511+2354	2017A&A...597A..79P	
J165601.6+211240	4564662075066830720	16 56 01.60	+21 12 41.1	2.24 ± 0.32	0.049	Sy1	LEDA1645221	2012ApJS..203...21A	
J170315.9+312725	1310317182535337216	17 03 15.72	+31 27 28.6	1.67 ± 0.42	0.034	LINER	Mrk700	1999PASP..111..438F	
J170922.4-0144010	4367895570106812544	17 09 22.40	-01 40 12.3	2.97 ± 0.58	0.093	Galaxy	2MASXJ17092228-0140124	2007MNRAS.375..931M	
J171228.4+355301	133838187327183488	17 12 28.43	+35 53 02.7	2.16 ± 0.48	0.026	Sy1	MCG+06-38-005	2012ApJS..203...21A	
J172239.8+305253	45977898162731008	17 22 39.93	+30 52 52.6	0.31 ± 0.07	0.043	Sy1	Mrk506	2012ApJS..203...21A	
J172533.0+571646	14328934875789984	17 25 33.08	+57 16 45.5	5.53 ± 1.16	0.066	Sy1	2MASXJ17253339+5716453	2012ApJS..203...21A	
J172608.1+743104	1655725217052044800	17 26 08.26	+74 31 04.0	1.78 ± 0.42	0.052	Sy1	2MASXJ17260822+7431043	1997A&A...320..395W	
J173629.5+174040	4550423468210659712	17 36 29.29	+17 40 39.6	3.68 ± 0.59	0.084	Galaxy	IRAS17342+1742	2000MNRAS.317...5S	
J174514.8+705128	1639075140673511424	17 45 14.77	+70 51 26.8	2.28 ± 0.49	0.272	Sy1	None	2022AstL...48..724K	
J174908.8+614030	1436218307661726976	17 49 09.10	+61 40 26.1	4.60 ± 1.17	0.039	Galaxy	2MASXJ17490910+6140262	1999PASP..111..438F	
J175505.5+651954	1440558727766378048	17 55 05.61	+65 19 55.0	0.73 ± 0.15	0.079	QSO	RXJ1755.0+6519	2003ApJS..149..296G	
J177510.9+475824	1363075598726822912	17 56 10.81	+47 58 24.8	2.49 ± 0.44	0.062	Sy2	None	2022AstL...48..724K	
J180203.5+290622	4584373913376142208	18 02 03.65	+29 06 20.9	3.27 ± 0.58	0.022	Galaxy	2MASXJ18020367+2906209	2003A&A...412..451P	
J181101.3+633323	2161443945276002176	18 11 00.99	+65 33 20.4	4.08 ± 0.51	0.050	Galaxy	2MASXJ18110093+6533203	2000ApJ...541..134X	
J181725.1+111849	4484513209326581824	18 17 25.15	+11 18 48.0	1.50 ± 0.40	0.058	AGN	2MASXJ18172518+1118475	2003A&A...412..451P	
J190050.5+284615	2040335556984894720	19 00 50.52	+28 46 16.4	4.10 ± 0.62	0.014	AGN	NGC6740	2003A&A...412..451P	
J190458.6+375541	209919327340753888	19 04 58.65	+37 55 41.0	0.70 ± 0.14	0.089	AGN	[MEB2011]KA11904+37	2012ApJ...751...52E	
J191734.8+451337	2127253875299563136	19 17 34.83	+45 13 37.2	0.87 ± 0.22	0.078	AGN	2MASXJ19173481+4513371	2018ApJ...857..141S	
J192156.1+550847	2140251786365419008	19 21 56.06	+55 08 47.1	3.30 ± 0.31	0.092	Sy2	None	2022AstL...48..724K	
J192852.3-251642	6766602609845906176	19 28 52.31	-25 16 38.7	5.20 ± 0.55	0.108	Galaxy	2MASXJ19285232-2516388	2009MNRAS.399..683J	
J193203.8+410244	2053551343150878336	19 32 04.02	+41 02 43.4	0.94 ± 0.20	0.083	Sy1	2MASXJ19320402+4102433	2022AstL...48..724K	
J195456.5-062851	4196937111313151744	19 54 56.43	-06 28 53.4	3.01 ± 0.28	0.029	Galaxy	2MASXJ19545644-0628535	2003A&A...412..451P	
J200751.1-110834	688090192879742112	20 07 51.30	-11 08 34.3	1.03 ± 0.25	0.031	Sy2	2MASXJ20075129-1108346	2009MNRAS.399..683J	
J202035.2+561501	2187638091826468352	20 20 35.21	+56 14 59.6	4.47 ± 0.51	0.034	Galaxy	2MASXJ20203523+5614596	2015ApJ...149..171T	
J203505.6+260330	185587241534318080	20 35 05.65	+26 03 29.9	0.70 ± 0.12	0.050	Sy1	LEDA140941	2014A&A...561A..67P	
J205812.4+300437	1858495678286706048	20 58 12.35	+30 04 37.2	0.82 ± 0.10	0.033	Sy1	2MASXJ1022164+1058159	2011MNRAS.416..2840L	
J210221.6+105816	17565558875119680	21 02 21.64	+10 58 16.0	2.39 ± 0.26	0.029	Sy1	FRL1170	2003A&A...412..451P	
J210317.7-343236	67803249959566304	21 03 17.88	-34 32 33.8	4.82 ± 0.82	0.071	Galaxy	1988MNRAS.233..691F	2014A&A...561A..67P	
J212400.3+340913	1855138731842796032	21 24 00.31	+34 09 11.6	0.97 ± 0.22	0.083	Sy1	2MASXJ124040483+3409114	2009MNRAS.399..683J	
J212404.9-164149	6835161283006507520	21 24 04.81	-16 41 48.1	7.01 ± 1.09	0.036	Galaxy SF	2MASXJ124040483-1641484	2011MNRAS.416..2840L	
J213833.4+320505	194676526202843494	21 38 33.43	+32 05 05.8	0.33 ± 0.07	0.025	Sy1	Z493-2		

Continuation of the table 1

SRG e+	GAIa EDR3+	RA	DEC	$\mu$ (mas/yr)	$\mu$	$z$	Type	Simbad	Reference
J214904.0-014111	2673969917489449088	21 49 03.97	-01 41 11.8	1.44 ± 0.26	0.053	QSO	6dFGSgJ214904.0-014112	2009MNRAS.399..638J	
J220509.5-004820	2677231034617335712	22 05 09.51	-00 48 20.5	4.16 ± 0.88	0.098	Sy1	2E2202.5-0103	2012ApJS..203...21A	
J222407.8+040912	2707307934677176960	22 24 07.82	+04 09 12.9	1.43 ± 0.37	0.098	AGN	2MASXJ22240782+0409124	2017ApJS..233...25A	
J222719.3+400549	1909278375151739264	22 27 19.04	+40 05 50.3	0.64 ± 0.11	0.068	QSO	2MASSJ22271903+4005502	2012ApJS..199...26H	
J223546.4-260302	6621415775889322880	22 35 46.20	-26 03 01.6	1.40 ± 0.22	0.005	Sy1	NGC7314	2004MNRAS.350.1195M	
J223655.9-221316	6627822939381980032	22 36 55.95	-22 13 15.0	0.58 ± 0.11	0.033	Sy1	ESO602-31	2009MNRAS.399..638J	
J223715.4+402943	1932429657626173184	22 37 15.51	+40 29 45.0	1.60 ± 0.23	0.058	AGN cand.	LEDA5060459	2012ApJS..199...26H	
J224017.2+080315	271579836346695328	22 40 17.06	+08 03 13.5	0.68 ± 0.13	0.025	Sy1	UGC12138	2018ApJ...861...49H	
J224156.0+201543	2834561493466339456	22 41 55.96	+20 15 41.4	1.58 ± 0.35	0.024	Sy	Mrk308	2018ApJ...861...49H	
J224311.1+032804	2704625950939055488	22 43 11.02	+03 28 04.8	0.84 ± 0.14	0.039	Galaxy	2MASXJ22431105+0328050	2012ApJS..199...26H	
J230812.1-281752	2379049803356498688	23 08 11.89	-28 17 52.9	2.84 ± 0.44	0.119	Galaxy	2dFGRSTGS187Z129	2001MNRAS.328.1039C	
J231119.5-265509	2379295853443238400	23 11 19.32	-26 55 08.4	2.40 ± 0.56	0.055	Galaxy	6dFGSgJ231119.3-265509	1998MNRAS.300..417R	
J231348.2+234918	28394529455822184960	23 13 48.31	+23 49 14.0	1.69 ± 0.45	0.021	Galaxy	Mrk317	2003A&A...412...45P	
J232009.8-293131	2329940253940761216	23 20 09.77	-29 31 30.0	0.56 ± 0.11	0.052	AGN cand.	LEDA13524	1998MNRAS.300..417R	
J232804.7+183153	2824026179208248064	23 28 04.84	+18 31 53.2	0.82 ± 0.20	0.023	Galaxy	MCG+03-59-058	2018ApJ...861...49H	
J232910.3+472800	1941757330160593536	23 29 10.44	+47 28 01.3	3.30 ± 0.55	0.040	Sy1	None	2022AstL...48..724K	
J233109.8-295746	2329256117190225152	23 31 09.79	-29 57 44.9	1.04 ± 0.35	0.053	Galaxy	2MASXJ23310975-2957452	1998MNRAS.300..417R	
J233515.6-085729	2438794099819112960	23 35 16.07	-08 57 23.5	5.23 ± 1.04	0.086	Galaxy	2MASXJ23351606-0857234	2012ApJS..203...21A	
J233523.0+450054	1937302143405657600	23 35 22.95	+45 00 54.5	0.58 ± 0.15	0.074	Galaxy	2MASXJ23352293+4500548	2000MNRAS.317...55S	
J233604.7-313450	2325865085891363200	23 36 04.96	-31 34 51.0	3.45 ± 0.75	0.062	Galaxy R	PKS2333-318	2007MNRAS.375..931M	
J233714.5-122123	2432491596089026688	23 37 14.39	-12 21 21.9	2.12 ± 0.49	0.101	Galaxy	6dFGSgJ233714.4-122122	1999MNRAS.308..897L	
J234726.2+505850	194417340388702592	23 47 26.32	+50 58 50.4	5.07 ± 0.83	0.062	Sy1	None	2022AstL...48..724K	
J234758.5-151241	241893469073325760	23 47 58.50	-15 12 41.9	2.48 ± 0.60	0.083	AGN	2MASXJ23475845-1512421	2007MNRAS.375..931M	
J235330.8+151256	2766655895853793664	23 53 30.74	+11 52 52.5	4.64 ± 0.68	0.235	QSO	SDSSJ235330.74+115252.4	2020ApJS..250...8L	
J235601.9+073123	274634018514738304	23 56 01.95	+07 31 23.3	2.13 ± 0.35	0.040	Sy1	Mrk541	2018ApJ...861...49H	
J235959.2+083354	2747061739653312768	23 59 59.30	+08 33 54.0	0.62 ± 0.09	0.083	Sy1	LEDA1349333	2000A&A...371.119.2540G	

Table 2: Catalog of extragalactic sources with significant proper motions - Seyfert galaxies of type 1.

RA (J2000)	DEC (J2000)	G (mag)	$\mu$ (mas/yr)	$\tau$	$X_v$	$L_X \times 10^{42}$ (erg/s)	z	$L_T \times 10^{42}$ (erg/s)
11 05 04.21	+50 59 49.9	19.86	9.43	-0.3	4.9	3.3	0.118	5.2
14 40 25.84	+33 27 02.6	20.82	9.41	-0.7	2.7	3.4	0.275	13.5
14 54 25.48	+46 45 24.1	18.99	8.99	0.1	5.2	5.7	0.069	3.3
13 56 20.70	+26 43 54.4	19.66	8.86	0.3	24.2	3.7	0.062	1.3
11 02 41.47	+42 06 51.9	19.35	7.02	-0.2	3.1	2.8	0.075	2.1
13 31 06.88	+51 09 30.9	20.15	6.85	-0.1	1.8	9.3	0.179	5.5
00 44 47.34	+15 29 11.9	20.22	6.51	-0.4	5.2	7.6	0.227	8.4
14 39 36.35	+44 55 04.3	19.29	6.03	0.1	5.2	8.4	0.088	2.6
17 25 33.08	+57 16 45.5	19.40	5.53	-0.5	5.3	1.1	0.066	1.2
15 24 33.35	+27 43 11.6	18.82	5.30	-0.6	2.4	1.4	0.069	1.8
23 47 26.32	+50 58 50.4	19.53	5.07	-0.1	10.8	1.7	0.062	0.7
14 48 19.38	+44 32 32.7	19.30	4.80	0.4	1.4	11.4	0.080	1.3
12 35 53.51	+42 41 21.0	20.09	4.44	-0.5	0.0	2.9	0.155	2.4
12 42 36.10	+78 07 20.4	18.24	4.30	0.1	2.9	1.1	0.022	0.2
14 11 09.17	+44 40 11.9	20.02	4.29	-0.6	3.7	0.9	0.095	0.9
15 17 51.71	+05 06 27.8	17.93	4.22	-0.1	3.6	3.3	0.039	1.0
15 33 44.60	+23 58 11.9	19.28	4.20	-0.8	9.1	0.6	0.067	0.9
22 05 09.51	-00 48 20.5	19.30	4.16	0.1	14.6	9.0	0.098	1.7
12 37 40.72	+61 11 48.6	19.79	4.10	-0.6	5.6	5.0	0.181	4.7
16 23 15.16	+34 28 24.1	19.99	3.96	-0.0	1.3	11.1	0.165	2.5
10 17 38.72	+42 01 03.3	18.91	3.94	-0.9	5.2	1.7	0.107	3.0
14 52 29.63	+38 34 24.7	19.44	3.76	-0.3	12.5	1.5	0.068	0.6
15 33 33.16	+32 18 13.5	19.66	3.68	0.2	15.9	3.7	0.065	0.5
02 12 57.60	+14 06 10.2	18.24	3.66	-0.1	5.3	6.7	0.062	1.7
14 37 31.70	+15 55 47.6	18.21	3.64	-1.0	16.9	0.3	0.037	0.5
14 12 38.15	+39 18 36.8	17.95	3.62	-0.6	1.9	0.4	0.026	0.3
15 44 50.38	+44 07 43.6	19.99	3.60	-0.7	3.3	7.2	0.255	7.3
16 29 21.83	+41 33 55.5	19.88	3.58	-0.2	9.1	8.5	0.161	2.7
07 25 28.48	+43 43 32.3	19.53	3.52	-0.4	4.6	1.3	0.069	0.6
11 17 05.21	+47 02 14.3	19.61	3.38	-0.3	6.1	11.3	0.188	4.2
11 39 25.56	+45 13 46.7	19.12	3.38	-0.5	11.0	5.5	0.127	3.2
23 29 10.44	+47 28 01.3	18.55	3.30	-1.2	2.3	0.1	0.040	0.4
00 28 48.78	+14 52 16.3	19.67	3.29	0.2	3.8	6.3	0.089	0.7
14 05 18.07	+17 49 14.4	19.27	3.26	-1.2	3.2	0.5	0.104	1.5
12 44 41.48	+37 40 25.1	19.72	3.24	-0.2	15.2	10.7	0.166	3.0
16 11 59.55	+31 10 41.5	19.65	3.23	0.0	4.0	17.0	0.159	3.0
13 14 47.07	+26 06 24.1	18.22	3.21	0.0	8.2	10.5	0.072	1.9
13 07 02.89	+56 31 58.4	18.86	3.09	-0.6	11.0	1.8	0.081	1.2
16 49 03.65	+19 03 07.1	19.51	3.05	-0.7	7.0	2.8	0.148	2.4
14 28 08.10	+46 42 03.3	19.28	3.04	0.1	11.6	5.3	0.074	0.7
12 06 55.63	+50 17 37.2	18.70	3.03	0.0	1.6	5.0	0.061	0.8
13 42 20.15	+38 42 09.7	19.06	3.02	0.3	3.1	11.4	0.079	0.9
15 23 45.08	+32 28 22.4	19.46	2.88	-1.3	0.0	0.2	0.077	0.7
13 44 48.63	+30 44 20.4	18.44	2.86	-0.4	28.0	4.3	0.077	1.7
13 58 30.78	+20 05 51.2	18.86	2.84	-1.3	2.4	0.2	0.062	0.7
16 18 18.49	+42 19 14.2	19.06	2.84	-0.5	12.1	9.9	0.165	4.8
02 10 49.38	+24 07 06.7	19.34	2.71	-1.0	4.3	1.6	0.144	2.3
10 11 48.35	+50 50 00.5	19.22	2.62	-0.3	15.7	2.7	0.079	0.7
03 20 06.32	+40 21 58.7	18.85	2.55	-0.3	18.2	1.3	0.047	0.3
14 55 17.69	+17 38 29.7	18.72	2.41	-0.3	2.6	5.9	0.095	1.5

Continuation of table 2 - Seyfert galaxies of type 1.

RA (J2000)	DEC (J2000)	G (mag)	$\mu$ (mas/yr)	$\tau$	$X_v$	$L_X \times 10^{42}$ (erg/s)	z	$L_T \times 10^{42}$ (erg/s)
21 02 21.64	+10 58 16.0	17.78	2.39	-0.1	14.9	1.9	0.029	0.3
14 46 40.21	+16 24 02.2	17.90	2.31	-0.8	2.4	1.2	0.054	0.9
17 45 14.77	+70 51 26.8	19.42	2.28	-0.5	1.7	18.5	0.272	7.0
16 56 01.60	+21 12 41.1	18.80	2.24	-0.0	1.4	2.7	0.049	0.3
16 14 56.18	+41 30 55.8	19.28	2.18	-1.0	2.6	3.2	0.196	3.6
17 12 28.43	+35 53 02.7	18.81	2.16	-1.2	2.4	0.04	0.026	0.08
23 56 01.95	+07 31 23.3	17.94	2.13	-1.1	7.8	0.3	0.040	0.4
11 23 48.04	+46 56 50.1	19.44	2.08	-0.2	2.5	12.3	0.157	2.1
12 17 45.79	+53 49 02.4	19.71	2.02	-0.4	4.3	9.0	0.194	2.4
04 05 51.36	+81 37 17.2	19.25	1.97	-0.4	6.5	4.6	0.118	1.2
13 38 26.87	+32 12 52.7	19.36	1.95	0.2	1.6	8.8	0.089	0.6
07 40 08.90	+80 03 57.1	18.73	1.91	0.1	2.9	11.4	0.087	0.9
17 26 08.26	+74 31 04.0	18.18	1.78	-0.5	2.2	2.0	0.052	0.6
02 04 36.76	-11 59 43.4	17.98	1.76	-0.4	5.3	5.8	0.073	1.3
16 25 01.44	+24 15 47.4	18.41	1.70	-0.6	25.6	1.1	0.050	0.4
16 19 44.98	+24 34 31.9	18.52	1.69	-0.0	7.4	6.4	0.065	0.6
12 44 12.06	+50 42 02.0	19.22	1.67	-0.2	14.7	28.5	0.216	3.8
09 21 08.59	+44 54 50.8	19.44	1.66	-0.0	16.2	18.0	0.156	1.5
09 04 36.95	+55 36 02.7	17.57	1.57	0.2	4.9	7.8	0.037	0.4
11 06 47.46	+72 34 07.3	15.36	1.57	-0.4	7.9	0.9	0.009	0.2
16 20 52.60	+54 00 58.6	18.69	1.54	-0.4	2.7	13.5	0.146	2.6
16 32 02.48	+32 03 39.4	18.80	1.53	-0.9	3.4	0.6	0.059	0.3
16 48 19.02	+30 22 10.8	18.30	1.48	-0.7	4.2	4.1	0.102	1.5
16 05 08.88	+32 39 21.5	18.82	1.48	-0.4	18.2	3.6	0.091	0.7
10 50 57.29	+59 32 14.5	18.40	1.41	-0.1	3.0	11.0	0.085	1.0
11 44 33.06	+61 32 00.7	18.56	1.41	-1.0	5.6	0.3	0.048	0.2
22 35 46.20	-26 03 01.6	17.72	1.40	0.4	1.8	0.2	0.005	0.005
14 47 39.33	+61 06 56.0	18.43	1.37	-1.1	3.5	2.6	0.137	2.3
10 22 33.70	+58 27 04.9	18.99	1.33	-0.1	5.0	4.7	0.077	0.4
11 29 57.95	+46 20 59.5	19.34	1.29	-0.3	12.1	21.2	0.210	2.7
12 31 52.05	+45 04 43.1	18.18	1.29	-0.4	5.3	3.3	0.062	0.5
13 03 01.05	+40 38 40.6	18.45	1.23	-0.6	11.7	1.8	0.067	0.4
11 09 19.75	+71 42 33.4	18.26	1.20	-0.3	2.2	19.8	0.130	2.3
05 35 32.13	+40 11 15.8	17.88	1.15	0.2	2.0	1.6	0.021	0.06
16 29 48.38	+67 22 42.0	17.90	1.14	-0.0	5.8	1.5	0.025	0.08
11 49 58.09	+57 51 07.7	18.72	1.06	-0.2	3.0	8.3	0.100	0.7
21 24 00.31	+34 09 11.6	18.82	0.97	0.0	5.7	9.3	0.083	0.4
19 32 04.02	+41 02 43.4	18.52	0.94	-0.2	2.1	7.1	0.083	0.5
13 10 56.19	+44 44 13.6	18.54	0.92	-0.4	24.7	2.1	0.060	0.2
13 49 15.20	+22 00 32.6	17.77	0.86	-0.7	2.9	2.1	0.062	0.4
12 34 29.86	+62 18 06.2	18.47	0.84	-0.3	1.5	15.8	0.135	1.3
20 58 12.35	+30 04 37.2	16.96	0.82	-0.2	1.3	4.1	0.033	0.3
12 46 12.11	+41 08 11.9	17.75	0.73	-0.3	2.8	6.5	0.067	0.5
20 35 05.65	+26 03 29.9	17.51	0.70	-0.0	3.2	8.9	0.050	0.3
22 40 17.06	+08 03 13.5	16.22	0.68	-0.4	2.6	2.8	0.025	0.2
15 08 52.81	+68 14 07.0	16.95	0.68	-0.1	2.2	17.3	0.058	0.7
14 34 52.46	+48 39 42.7	18.03	0.68	-0.3	8.0	1.6	0.037	0.1
12 16 07.10	+50 49 30.1	17.36	0.67	-0.1	5.2	3.4	0.031	0.1
15 20 43.23	+30 41 22.6	18.06	0.65	-0.1	5.1	12.2	0.077	0.5
23 59 59.30	+08 33 54.0	17.40	0.62	-0.0	2.1	30.2	0.083	0.9
13 20 24.61	+69 00 11.6	17.74	0.61	-0.1	1.5	10.7	0.067	0.4
22 36 55.95	-22 13 15.0	16.88	0.58	-0.2	5.7	4.6	0.033	0.2

Continuation of table 2 - Seyfert galaxies of type 1.

RA (J2000)	DEC (J2000)	G (mag)	$\mu$ (mas/yr)	$\tau$	$X_v$	$L_X \times 10^{42}$ (erg/s)	z	$L_T \times 10^{42}$ (erg/s)
14 26 30.68	+39 03 43.4	17.15	0.51	-0.2	2.0	22.6	0.081	0.9
21 38 33.43	+32 05 05.8	16.05	0.33	-0.2	2.4	5.1	0.025	0.1
13 42 08.38	+35 39 15.5	16.27	0.32	-1.3	8.1	0.006	0.003	0.002
17 22 39.93	+30 52 52.6	16.75	0.31	0.0	4.6	15.4	0.043	0.2

Table 3: Catalog of extragalactic sources with significant proper motions - Seyfert galaxies of type 2.

RA (J2000)	DEC (J2000)	G (mag)	$\mu$ (mas/yr)	$\tau$	$X_v$	$L_X \times 10^{42}$ (erg/s)	z	$L_T \times 10^{42}$ (erg/s)
16 08 51.07	+29 57 15.0	19.91	9.98	-0.9	0.0	0.1	0.048	0.8
16 53 15.06	+23 49 42.9	19.58	8.61	-1.1	0.0	0.6	0.103	4.7
14 16 07.75	+35 20 37.8	17.99	6.75	-1.4	4.7	0.02	0.013	0.2
12 46 17.34	+28 20 33.9	19.13	5.35	-0.6	5.9	2.4	0.100	3.1
13 15 17.26	+44 24 25.5	18.71	5.33	-0.8	6.1	0.2	0.035	0.5
06 52 36.99	+45 46 50.2	18.08	4.90	-1.5	2.6	0.03	0.021	0.3
14 23 07.51	+28 35 42.3	18.21	4.25	-0.9	3.7	0.2	0.029	0.4
14 08 45.73	+35 32 18.6	19.27	3.60	-1.3	0.0	1.3	0.166	5.1
12 16 51.77	+37 54 38.1	18.44	3.50	-0.0	3.1	6.3	0.063	1.2
03 25 12.95	+40 41 52.8	18.85	3.45	-0.4	2.4	1.1	0.047	0.5
10 16 53.65	+73 24 02.7	17.72	3.44	-0.1	1.3	0.2	0.009	0.05
01 08 11.86	+85 41 50.7	19.39	3.35	-0.4	7.4	1.6	0.077	0.8
13 48 34.95	+26 31 09.9	17.95	3.31	0.0	1.8	9.7	0.059	1.8
19 21 56.06	+55 08 47.1	18.36	3.30	-0.9	1.2	2.2	0.092	3.1
15 56 40.32	+45 13 38.4	19.75	3.09	-0.4	1.9	7.9	0.181	3.3
14 30 16.04	+23 03 44.5	19.09	3.05	0.5	9.6	20.8	0.081	1.1
15 45 29.63	+25 11 27.9	19.13	2.82	-0.1	7.0	9.9	0.117	1.9
17 56 10.81	+47 58 24.8	18.67	2.49	-1.1	1.5	0.4	0.062	0.6
13 28 11.58	+62 27 43.0	19.25	2.33	-0.6	2.5	1.8	0.091	0.9
13 04 22.19	+36 15 43.2	17.80	2.31	-1.6	0.0	0.1	0.045	0.7
13 38 04.30	+39 41 10.1	19.24	2.16	-0.3	33.5	1.5	0.060	0.3
14 28 17.99	+57 10 18.5	17.83	2.05	-1.1	1.4	0.4	0.043	0.5
13 31 47.08	+59 10 47.2	17.70	2.01	-0.2	7.2	3.9	0.043	0.6
16 51 21.88	+21 55 26.3	18.52	2.01	-1.5	0.0	0.2	0.055	0.5
13 53 17.80	+33 29 27.0	18.00	2.01	-1.5	2.3	0.004	0.008	0.01
00 03 10.02	+04 44 56.2	18.15	1.94	-1.3	2.8	0.4	0.058	0.8
02 44 43.31	+20 41 38.6	18.68	1.79	-0.4	29.6	1.2	0.051	0.3
01 25 31.46	+32 08 10.5	17.23	1.62	0.3	4.2	2.6	0.016	0.1
13 54 19.95	+32 55 47.7	18.14	1.50	-0.2	2.1	0.9	0.026	0.1
10 41 19.22	+57 45 00.1	17.51	1.13	-1.8	0.0	0.3	0.068	1.0
14 14 15.18	+26 44 51.4	16.69	1.06	-1.7	5.6	0.2	0.035	0.5
20 07 51.30	-11 08 34.3	17.96	1.03	-0.2	8.3	1.4	0.031	0.1

Table 4: Catalog of extragalactic sources with significant proper motions - AGN of undetermined type.

RA (J2000)	DEC (J2000)	G (mag)	$\mu$ (mas/yr)	$\tau$	$X_v$	$L_X \times 10^{42}$ (erg/s)	z	$L_T \times 10^{42}$ (erg/s)
14 19 43.23	+49 14 11.9	17.35	6.10	-1.8	2.4	0.04	0.026	1.0

Continuation of the table 4 - AGN of undetermined type.

RA (J2000)	DEC (J2000)	G (mag)	$\mu$ (mas/yr)	$\tau$	$X_v$	$L_X \times 10^{42}$ (erg/s)	z	$L_T \times 10^{42}$ (erg/s)
14 43 31.26	+49 23 35.2	18.93	5.82	-0.2	5.7	0.6	0.030	0.4
00 11 24.46	+38 09 33.7	19.92	5.72	-0.4	4.4	3.8	0.137	3.5
06 23 29.08	+69 12 32.6	19.93	4.54	-0.6	2.9	0.3	0.055	0.4
05 38 23.46	+79 35 12.7	17.53	4.27	-2.1	0.0	0.007	0.015	0.2
15 39 37.06	+59 19 55.2	19.26	4.13	-0.8	1.6	0.009	0.008	0.01
01 20 48.01	-08 29 18.4	18.69	4.10	-0.5	2.6	0.5	0.034	0.3
19 00 50.52	+28 46 16.4	18.95	4.10	-0.4	9.3	0.08	0.014	0.05
14 38 21.17	+46 49 43.7	20.37	4.02	-0.9	0.0	5.0	0.324	9.1
04 41 11.00	+68 37 29.3	19.78	3.87	-0.1	2.0	6.0	0.120	1.7
08 04 35.51	+50 42 30.7	19.28	3.71	-1.1	0.0	0.03	0.023	0.07
01 10 14.06	+50 10 31.0	18.96	2.81	-0.2	1.4	0.4	0.024	0.09
23 47 58.50	-15 12 41.9	18.78	2.48	-0.2	5.7	5.2	0.083	1.1
13 43 52.89	+80 35 49.4	18.67	2.46	-0.0	1.8	2.5	0.045	0.3
13 20 37.89	+34 11 26.2	18.88	2.44	-0.7	6.7	0.9	0.064	0.6
06 31 47.43	+65 54 42.5	19.36	1.97	-0.7	5.1	1.6	0.108	0.8
09 50 33.15	+44 18 51.6	17.89	1.76	-0.5	1.4	0.2	0.016	0.06
22 37 15.51	+40 29 45.0	18.43	1.60	0.3	2.8	10.4	0.058	0.4
22 41 55.96	+20 15 41.4	16.75	1.58	-2.1	0.0	0.03	0.024	0.3
18 17 25.15	+11 18 48.0	18.32	1.50	-0.0	2.6	5.8	0.058	0.4
22 24 07.82	+04 09 12.9	18.28	1.43	0.3	3.4	38.2	0.098	1.4
10 59 46.68	+45 54 09.7	19.16	1.39	-0.4	9.3	12.0	0.179	2.1
19 17 34.83	+45 13 37.2	17.40	0.87	-0.7	2.5	5.8	0.078	1.2
19 04 58.65	+37 55 41.0	17.37	0.70	-0.7	2.2	7.7	0.089	1.3
23 20 09.77	-29 31 30.0	16.96	0.56	-0.3	2.2	9.2	0.052	0.5

Table 5: Catalog of extragalactic sources with significant proper motions - LINER-type AGNs.

RA (J2000)	DEC (J2000)	G (mag)	$\mu$ (mas/yr)	$\tau$	$X_v$	$L_X \times 10^{42}$ (erg/s)	z	$L_T \times 10^{42}$ (erg/s)
09 11 18.96	+46 23 07.2	19.43	7.93	-0.3	8.1	3.8	0.103	4.4
16 13 18.50	+36 16 21.9	19.80	7.71	-1.2	2.4	0.2	0.082	1.7
09 05 54.50	+47 10 45.5	18.74	4.08	-1.0	3.2	0.08	0.027	0.2
15 53 40.36	+43 44 04.9	19.25	4.06	-0.2	2.4	0.8	0.040	0.3
12 02 15.46	+44 03 19.7	19.65	3.80	-0.1	8.9	4.3	0.101	1.2
16 51 29.52	+19 24 59.9	18.30	3.61	-0.8	3.7	0.1	0.023	0.2
12 10 49.61	+39 28 22.1	18.32	3.54	-0.4	24.8	0.4	0.022	0.2
14 33 18.48	+34 44 04.4	18.93	3.06	-0.5	1.9	0.3	0.034	0.2
13 43 30.01	+51 02 04.1	19.70	2.93	0.3	4.1	17.7	0.131	1.4
11 22 17.90	+59 04 28.3	17.74	1.88	-0.9	10.2	0.008	0.005	0.006
17 03 15.72	+31 27 28.6	17.04	1.67	-1.6	1.7	0.2	0.034	0.6

Table 6: Catalog of extragalactic sources with significant proper motions - quasars.

RA (J2000)	DEC (J2000)	G (mag)	$\mu$ (mas/yr)	$\tau$	$X_v$	$L_X \times 10^{42}$ (erg/s)	z	$L_T \times 10^{42}$ (erg/s)
13 11 18.54	+46 35 02.3	19.45	14.94	-0.3	2.4	28.4	0.271	130.3
01 44 17.27	+31 40 03.3	20.09	9.32	-0.2	6.6	3.5	0.124	4.2

Continuation of the table 6 - quasars.

RA (J2000)	DEC (J2000)	G (mag)	$\mu$ (mas/yr)	$\tau$	$X_v$	$L_X \times 10^{42}$ (erg/s)	z	$L_T \times 10^{42}$ (erg/s)
23 53 30.74	+11 52 52.5	20.06	4.64	0.1	2.2	29.8	0.235	6.6
00 50 55.69	+29 33 28.1	19.63	4.56	-0.5	5.8	3.3	0.136	2.8
01 34 35.91	+02 28 39.9	19.32	3.51	-0.2	8.6	15.5	0.177	4.8
14 49 24.44	+32 18 16.2	18.37	3.29	-0.3	5.9	2.6	0.058	1.0
15 09 08.76	+09 02 21.0	18.31	2.65	-1.5	0.0	0.1	0.044	0.6
14 37 01.50	+26 40 19.2	19.06	2.08	0.0	3.1	56.3	0.218	6.0
21 49 03.97	-01 41 11.8	18.24	1.44	0.0	3.3	5.7	0.053	0.4
17 55 05.61	+65 19 55.0	17.32	0.73	-0.1	2.1	21.2	0.079	0.9
22 27 19.04	+40 05 50.3	17.42	0.64	-1.0	6.4	2.0	0.068	0.6

Table 7: Catalog of extragalactic sources with significant proper motions - blazars.

RA (J2000)	DEC (J2000)	G (mag)	$\mu$ (mas/yr)	$\tau$	$X_v$	$L_X \times 10^{42}$ (erg/s)	z	$L_T \times 10^{42}$ (erg/s)
16 40 58.89	+11 44 04.2	18.00	2.05	-0.4	1.6	6.0	0.078	1.6
07 52 44.21	+45 56 57.4	18.17	1.29	-0.1	2.1	4.6	0.052	0.4

Table 8: Catalog of extragalactic sources with significant proper motions - radio galaxies.

RA (J2000)	DEC (J2000)	G (mag)	$\mu$ (mas/yr)	$\tau$	$X_v$	$L_X \times 10^{42}$ (erg/s)	z	$L_T \times 10^{42}$ (erg/s)
12 43 11.22	+73 15 59.3	19.06	4.96	-0.2	2.4	3.3	0.075	1.6
01 19 59.60	+14 47 10.4	17.11	4.83	-1.9	3.1	0.01	0.014	0.3
15 22 40.24	+31 08 56.7	19.02	4.32	-0.9	5.2	1.9	0.116	3.8
23 36 04.96	-31 34 51.0	19.06	3.45	-0.4	1.5	1.3	0.062	0.6

Table 9: Catalog of extragalactic sources with significant proper motions - star-forming galaxies.

RA (J2000)	DEC (J2000)	G (mag)	$\mu$ (mas/yr)	$\tau$	$X_v$	$L_X \times 10^{42}$ (erg/s)	z	$L_T \times 10^{42}$ (erg/s)
15 17 22.00	+46 58 12.9	20.61	17.63	-0.5	3.1	2.2	0.154	27.8
15 13 45.76	+31 11 25.1	20.48	7.37	-0.4	5.1	0.5	0.072	0.7
21 24 04.81	-16 41 48.1	19.17	7.01	-0.8	0.0	0.2	0.036	0.5
12 35 02.66	+66 22 33.5	18.22	5.41	-1.7	0.0	0.09	0.047	1.5
14 54 04.58	+36 33 20.5	19.79	5.20	-0.8	5.6	0.4	0.071	0.7
13 36 50.95	+36 50 18.0	18.76	5.15	-0.6	1.6	1.2	0.062	1.5
15 14 44.82	+26 54 32.5	19.96	5.12	-0.3	5.0	4.0	0.138	2.5
14 42 27.61	+55 58 46.4	18.61	4.61	-1.2	1.6	0.5	0.077	2.2
13 00 40.78	+52 32 15.8	18.73	4.20	-0.5	17.3	1.3	0.054	1.0
14 42 14.63	+29 18 08.9	19.46	3.78	-0.7	6.1	0.5	0.062	0.5
00 34 15.47	-27 48 12.7	17.15	3.69	-1.3	6.0	0.006	0.005	0.03
15 08 42.62	+28 10 16.2	18.22	3.65	-1.8	2.1	0.02	0.026	0.3
14 12 22.83	+33 57 15.5	20.04	3.36	-0.3	2.3	2.7	0.116	1.0
15 59 43.94	+27 42 29.7	18.69	3.04	-1.8	0.0	0.06	0.051	0.6
13 29 45.92	+55 36 13.4	17.85	1.35	-1.7	0.0	0.01	0.017	0.05

Continuation of the table 9 - star-forming galaxies.

RA (J2000)	DEC (J2000)	G (mag)	$\mu$ (mas/yr)	$\tau$	$X_v$	$L_X \times 10^{42}$ (erg/s)	z	$L_T \times 10^{42}$ (erg/s)
------------	-------------	------------	-------------------	--------	-------	---------------------------------	---	---------------------------------

Table 10: Catalog of extragalactic sources with significant proper motions - galaxies with undetermined type.

RA (J2000)	DEC (J2000)	G (mag)	$\mu$ (mas/yr)	$\tau$	$X_v$	$L_X \times 10^{42}$ (erg/s)	z	$L_T \times 10^{42}$ (erg/s)
04 31 22.51	+60 55 00.2	18.49	7.50	-1.5	0.0	0.010	0.015	0.2
05 08 09.16	+70 05 30.1	19.40	5.93	-0.3	2.6	0.2	0.028	0.2
16 24 33.47	+55 54 52.6	18.54	5.73	-1.7	2.1	0.03	0.031	0.6
16 52 51.42	+17 26 51.0	19.16	5.68	0.5	4.7	2.7	0.034	0.3
16 32 20.70	+64 10 53.5	19.15	5.31	-1.4	2.5	0.1	0.065	1.2
23 35 16.07	-08 57 23.5	20.04	5.23	-0.7	0.0	0.6	0.086	1.0
19 28 52.31	-25 16 38.7	19.17	5.20	-0.9	2.0	1.4	0.108	3.5
05 13 16.43	+66 27 50.2	19.06	5.12	-0.2	2.4	0.1	0.015	0.05
02 25 33.77	+26 44 01.7	18.32	4.86	-1.1	8.5	0.2	0.035	0.6
21 03 17.88	-34 32 33.8	19.44	4.82	-0.3	8.5	1.6	0.071	0.9
17 49 09.10	+61 40 26.1	19.63	4.60	-1.4	2.3	0.03	0.039	0.2
20 20 35.21	+56 14 59.6	18.96	4.47	-0.1	32.6	0.9	0.034	0.3
01 49 18.04	+85 15 37.2	19.33	4.15	-1.4	0.0	0.0004	0.004	0.003
18 11 00.99	+65 33 20.4	18.96	4.08	-2.0	2.1	0.03	0.050	0.6
11 51 06.87	+55 04 43.4	16.15	3.85	-2.0	3.4	0.05	0.020	1.0
00 29 36.79	-17 38 30.4	17.67	3.85	-0.4	9.5	4.1	0.054	2.2
17 36 29.29	+17 40 39.6	18.26	3.68	-1.5	1.6	0.5	0.084	3.2
16 35 09.19	+46 12 50.1	19.04	3.65	-1.2	3.6	0.05	0.031	0.2
06 37 09.94	+53 53 46.1	17.92	3.41	-1.5	0.0	0.09	0.034	0.6
18 02 03.65	+29 06 20.9	18.77	3.27	-1.4	2.0	0.02	0.022	0.10
00 32 46.03	-19 39 30.4	18.91	3.12	-1.4	0.0	0.1	0.054	0.5
11 32 34.85	+53 04 04.5	18.24	3.01	-0.4	2.0	0.007	0.003	0.003
19 54 56.43	-06 28 53.4	17.32	3.01	-0.9	2.0	0.4	0.029	0.6
00 38 26.67	-00 00 42.7	18.23	2.99	-1.5	1.4	0.1	0.045	0.6
01 42 38.57	-04 51 41.1	19.23	2.98	-1.3	0.0	0.06	0.040	0.2
17 09 22.40	-01 40 12.3	19.46	2.97	0.1	5.8	7.4	0.093	0.9
01 08 16.31	-11 34 01.0	18.63	2.85	-0.2	2.5	1.7	0.047	0.4
23 08 11.89	-28 17 52.9	18.64	2.84	-0.2	23.6	12.4	0.119	3.0
02 40 12.22	-02 33 44.4	18.45	2.73	-0.1	5.8	2.4	0.043	0.4
07 06 34.82	+63 50 56.1	18.00	2.58	-0.5	8.4	0.1	0.014	0.06
23 11 19.32	-26 55 08.4	19.23	2.40	-0.2	7.5	1.4	0.055	0.3
23 37 14.39	-12 21 21.9	17.86	2.12	-0.8	1.4	4.9	0.101	3.4
01 44 58.56	-02 31 59.0	17.73	1.98	-0.0	4.7	28.5	0.096	2.9
23 13 48.31	+23 49 14.0	17.91	1.69	-1.2	6.1	0.07	0.021	0.10
02 37 59.99	+19 38 11.8	18.75	1.68	0.3	6.3	2.5	0.034	0.1
16 43 13.78	+09 54 16.2	17.33	1.63	-0.1	3.0	8.2	0.047	0.8
01 17 11.23	-22 09 03.6	18.19	1.52	-0.5	1.8	5.1	0.090	1.2
23 31 09.79	-29 57 44.9	18.48	1.04	-0.3	32.3	2.1	0.053	0.2
07 25 46.68	+53 11 59.1	18.13	0.94	-0.2	5.8	2.2	0.039	0.2
22 43 11.02	+03 28 04.8	17.15	0.84	-0.9	22.8	1.1	0.039	0.4
23 28 04.84	+18 31 53.2	17.60	0.82	-0.2	3.7	1.3	0.023	0.08
23 35 22.95	+45 00 54.5	17.82	0.58	-0.8	16.0	2.3	0.074	0.4